

# Magma plumbing beneath Anak Krakatau volcano, Indonesia: evidence for multiple magma storage regions

Börje Dahren · Valentin R. Troll · Ulf B. Andersson ·  
Jane P. Chadwick · Màiri F. Gardner ·  
Kairly Jaxybulatov · Ivan Koulakov

Received: 10 December 2010 / Accepted: 2 September 2011  
© Springer-Verlag 2011

**Abstract** Understanding magma plumbing is essential for predicting the behaviour of explosive volcanoes. We investigate magma plumbing at the highly active Anak Krakatau volcano (Indonesia), situated on the rim of the 1883 Krakatau caldera by employing a suite of thermobarometric models. These include clinopyroxene-melt thermobarometry, plagioclase-melt thermobarometry, clinopyroxene composition barometry and olivine-melt thermometry. Petrological studies have previously identified shallow magma storage in the region of 2–8 km beneath Krakatau, while existing seismic evidence points towards mid- to deep-crustal storage zone(s), at 9 and 22 km, respectively. Our results show that

clinopyroxene in Anak Krakatau lavas crystallized at a depth of 7–12 km, while plagioclase records both shallow crustal (3–7 km) and sub-Moho (23–28 km) levels of crystallization. These magma storage regions coincide with well-constrained major lithological boundaries in the crust, implying that magma ascent and storage at Anak Krakatau is strongly controlled by crustal properties. A tandem seismic tomography survey independently identified a separate upper crustal (<7 km) and a lower to mid-crustal magma storage region (>7 km). Both petrological and seismic methods are sensitive in detecting magma bodies in the crust, but suffer from various limitations. Combined geophysical and petrological surveys, in turn, offer increased potential for a comprehensive characterization of magma plumbing at active volcanic complexes.

Communicated by J. Hoefs.

**Electronic supplementary material** The online version of this article (doi:10.1007/s00410-011-0690-8) contains supplementary material, which is available to authorized users.

B. Dahren (✉) · V. R. Troll · U. B. Andersson  
Department of Earth Sciences, CEMPEG,  
Uppsala University, Uppsala, Sweden  
e-mail: borje.dahren@geo.uu.se

U. B. Andersson  
Research Department, Swedish Museum of Natural History,  
Stockholm, Sweden

J. P. Chadwick  
Department of Petrology, Vrije Universiteit Amsterdam,  
Amsterdam, The Netherlands

M. F. Gardner  
Department of Geology,  
University College Cork, Cork, Ireland

K. Jaxybulatov · I. Koulakov  
Institute for Petroleum Geology and Geophysics,  
SB RAS, Novosibirsk, Russia

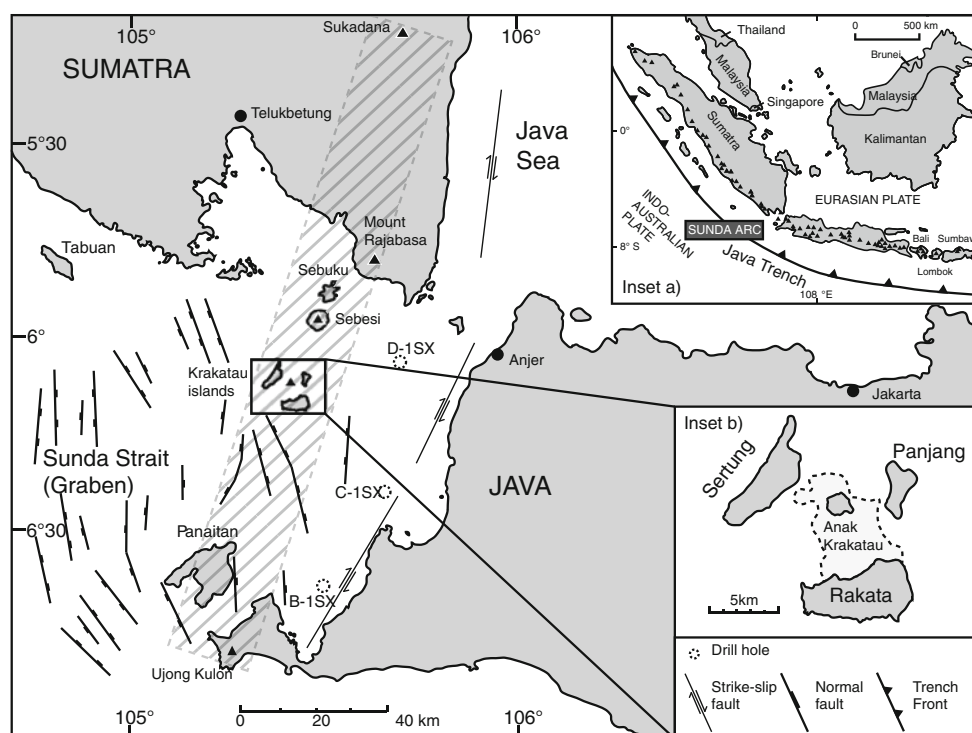
**Keywords** Anak Krakatau · Thermobarometry ·  
Clinopyroxene · Plagioclase · Magma plumbing · Seismic  
tomography

## Introduction

The Krakatau volcanic complex (Fig. 1), western Java (Indonesia), is one of the most infamous volcanoes worldwide due to the caldera-forming eruption of 1883 during which Krakatau Island collapsed into the sea. Inside the remnants of the old structure, a new volcanic cone breached the ocean surface in 1927, earning the name Anak Krakatau, “child of Krakatau” (Stehn 1929).

The bimodal nature of the Krakatau complex, i.e. extended periods of basalt and/or basaltic andesite eruptions developing towards, and culminating in, colossal high-silica caldera-forming ignimbrite eruptions, was originally noted by van Bemmelen (1949). The topic has

**Fig. 1** Simplified geological and structural map of the Sunda Straits, based on Mandeville et al. (1996a), Schlüter et al. (2002), Lunt et al. (2009) and Susilohadi et al. (2009). The locations of volcanoes that together with Anak Krakatau define a north–south trending volcanic lineament are marked with *triangles*. The hatched area in the centre represents the volcanic lineament of quaternary volcanoes discussed in Nishimura and Harjono (1992). *Inset a* shows location relative to regional geography and the boundary between the subducting Indo-Australian plate and the Eurasian Plate. *Inset b* shows details of Krakatau volcano



been further discussed by other authors (e.g. Camus et al. 1987; Mandeville et al. 1996a), but still lacks a comprehensive treatment. Improved knowledge of the magma plumbing system beneath Anak Krakatau will improve our understanding and better allow for prediction of future activity at this highly dynamic volcanic complex.

The aim of this investigation is therefore to constrain the current depth of magma storage region(s) beneath Anak Krakatau. We approach this problem by employing pressure and temperature modelling calculations that use measured mineral and rock composition data and calibrated thermodynamic formulations. The focus will be on clinopyroxene-melt and plagioclase-melt thermobarometry (Putirka et al. 2003; Putirka 2005, 2008), but data derived from the application of these thermobarometers will be compared with those obtained from clinopyroxene composition barometry and olivine-melt thermometry (Nimis 1999; Putirka et al. 2007; Putirka 2008). The mineral data set consists of electron microprobe (EMP) and X-ray fluorescence (XRF) analyses of minerals and rocks erupted between 1883 and 2002. The results will serve as an independent test of previous estimates and constraints on magma storage derived by geophysical means, plagioclase-melt geobarometry and in situ isotope stratigraphy (Camus et al. 1987; Harjono et al. 1989; Mandeville et al. 1996a; Gardner et al. 2006, *in press*). Our thermobarometric approach will be integrated with the results of a geophysical survey, using local earthquake tomographic inversion, aimed at investigating the seismic structure beneath the

Krakatau volcanic complex and surrounding areas (Hoffmann-Rothe et al. 2006; Jaxybulatov et al. 2011).

Our study applies, for the first time, barometry based on clinopyroxene to provide an independent and complementary test to isotopic, geophysical and geobarometric depth constraints for Anak Krakatau.

### Geotectonic setting

The Krakatau archipelago lies in the Sunda arc where the Indo-Australian plate is subducted beneath the Eurasian one (Fig. 1, inset a). In west Java, subduction is occurring at a rate of  $67 \pm 7$  mm per year (Tregoning et al. 1994). The Sunda arc is an active volcanic region, with the Krakatau volcanic complex being one of the most active parts. Since 1927, when it emerged above sea level, Anak Krakatau has had numerous eruptions and has grown to a height of  $\sim 315$  m (Hoffmann-Rothe et al. 2006), which translates to an average growth rate of  $\sim 7.5$  cm per week. The contemporary Krakatau archipelago and volcanic complex consists of four islands; Rakata, Sertung, Panjang and Anak Krakatau. The only exposed remnant of the pre-1883 edifice of Krakatau is the dissected cone of Rakata, previously the southernmost peak of the pre-1883 volcanic complex. The submarine caldera formed in the 1883 eruption is visible as a  $\sim 100$ -m-deep depression in the sea floor (Deplus et al. 1995). Although presently largely covered with 1883 eruptive products, the islands of Sertung

and Panjang are remnants of an earlier “proto-Krakatau” eruption. The records in local Javanese folk stories, e.g. the Book of Kings, or ‘Pararaton’ (Judd 1889; Nishimura et al. 1986; Camus et al. 1987), describe heavy rains of stone in the year 338 Saka (416 AD). While there is no direct evidence for an eruption of this size at that time, it may be a mistaken date for another eruption in 535 AD (Wohletz 2000). In addition, there is evidence for a yet older large ignimbrite eruption at  $\sim 60,000$  BC (Ninkovich 1979), indicating a cyclic nature to behaviour of the Krakatau complex.

The Krakatau volcanic complex as a whole is part of a NNE-SSW trending lineament of quaternary volcanic edifices, which lies approximately perpendicular to the Java trench (Nishimura and Harjono 1992) (Fig. 1). This lineament is related to a north–south trending fracture zone that is manifested in a shallow seismic belt with foci depths predominantly in the range of 0–20 km (Harjono et al. 1989; Nishimura and Harjono 1992; Špičák et al. 2002). Furthermore, the Krakatau volcanic complex is located at the intersection of this volcanic lineament and a fault connecting Krakatau to the Sunda Strait graben (Harjono et al. 1989; Deplus et al. 1995). In fact, the whole of the Sunda Strait is subject to extensive faulting and extensional rifting, attributed to the clockwise rotation of Sumatra relative to Java by  $\sim 20^\circ$  since the late Cenozoic (Ninkovich 1976; Nishimura et al. 1986; Harjono et al. 1991; Schlüter et al. 2002). The angle of plate convergence changes from near perpendicular ( $13^\circ$ ) in front of Java to oblique ( $55^\circ$ ) in front of Sumatra (Jarrard 1986). The Sumatran rotation has resulted in extensional thinning of the crust to  $\sim 20$  km in the Sunda Strait, as compared to 25–30 km in Sumatra and west Java (Harjono et al. 1991; Nishimura and Harjono 1992). The micro-seismic study by Harjono et al. (1989) estimated the crustal thickness directly below Anak Krakatau to be  $\sim 22$  km.

The influence of the rifting is manifested in Sukadana (Fig. 1), where 0.8–1.2 Ma MORB-type basalts are found (Nishimura and Harjono 1992). The magmatism in the Sunda Strait is thus not exclusively subduction zone related, but can also be a function of extensional tectonics.

Drill cores obtained during hydrocarbon exploration by Pertamina/Aminoil provide information on the bedrock at depth in the Sunda Strait (Noujiam 1976; Mandeville et al. 1996a). The closest of these drilled wells (C-1SX) is located  $\sim 30$  km southeast of Anak Krakatau (Fig. 1). The C-1SX well penetrated a sequence of sediments and sedimentary rocks of Quaternary to Upper Pliocene age. The upper part (0–600 m) consists of unconsolidated marine clays followed by clay-dominated siliciclastic rocks interbedded with volcanoclastic material to a depth of at least 3,000 m (Nishimura and Harjono 1992; Mandeville et al. 1996a). Findings by Lelgemann et al. (2000) suggest that

the extension and rapid subsidence of the Sunda Strait have created space for up to 6 km of graben fill. Thus, the total depth of the sediments and sedimentary rocks in this part of the Sunda Straits can be constrained to between 3 and 6 km. The Pertamina-Aminoil wells all failed to reach the basement below the sedimentary sequence, but other wells to the southeast of Sumatra and northwest of Java have drilled Cretaceous granites and quartz-monzonites (Hamilton 1979). The assumption of a sedimentary sequence underlain by a plutonic basement below Krakatau (Harjono et al. 1991) is supported by the presence of sedimentary (Mandeville et al. 1996b; Gardner et al. *in press*), granitic (Ōba et al. 1983) as well as dioritic, gabbroic and meta-basic xenoliths (Ōba et al. 1983; Gardner et al. *in press*) in Krakatau lavas and pyroclastic flows. The micro-seismic study by Harjono et al. (1989) identified three boundaries in the crust below the Krakatau complex, with unique crustal velocities, which should correspond with lithological boundaries (Fig. 2). The upper boundary (4 km) very likely represents the sedimentary-plutonic transition. The boundary at 9 km represents a density contrast that implies a change in lithology from low-density (e.g. granite)- to a higher-density plutonic rock (e.g. diorite or gabbro) and the lowermost boundary at 22 km represents the Moho.

#### Whole rock geochemistry

Figure 3 shows whole rock geochemistry of lava flows, bombs and ash erupted from Krakatau and Anak Krakatau

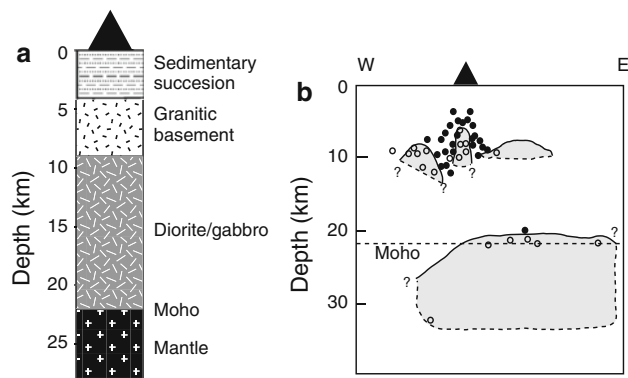


**Fig. 2** **a** Inferred stratigraphy of the bedrock below Anak Krakatau. The lithologies are constrained by data obtained from xenoliths (Ōba et al. 1983; Camus et al. 1987; Mandeville et al. 1996b; Gardner et al. *in press*), drill holes and seismic studies (Harjono et al. 1989; Kopp et al. 2001). **b** Cross-section through the crust showing seismic attenuation zones detected below Anak Krakatau (redrawn from Harjono et al. 1989). Circles represent earthquake foci with (*open circles*) and without (*filled circles*) S-wave attenuation. The inferred magma storage regions are represented by the *grey shapes*. Note that a lack of data from the lower crust in this study meant that it was not possible to decide whether or not these two attenuation zones are connected

in terms of total alkalis versus silica (TAS). Data are taken from Zen and Hadikusumo (1964), Self (1982), Camus et al. (1987), Mandeville et al. (1996a) and Gardner et al. (2006, *in press*). All oxide values have been normalized to 100% (volatile free), and iron content is FeO<sub>t</sub>. Note that the lava flows and bombs of the 1990–2002 described in Gardner et al. (2006; *in press*) are the same samples that are used for the petrographic and microprobe analyses in this study. Analyses of rocks erupted during the 1883 rhyodacitic eruption and between 1960 and 1981 at Anak Krakatau are also plotted in Fig. 3.

The rocks plot in two main groups in the TAS diagram. The pumices and obsidians of the 1883 eruption plot in the dacite-rhyolite field, while the lava flows and bombs from Anak Krakatau belong to a rather homogenous suite of basaltic andesites. The exceptions to this would be the 1960–1963 and 1981 eruptions (basalts and acidic-andesites, respectively), but these seem to represent isolated events with anomalous chemistry compared with the majority of eruptions. Note also that several basaltic dyke rocks from the island of Rakata with a similar composition to the 1963 basaltic flows have been reported (Camus et al. 1987). The early history of Anak Krakatau is, unfortunately, not well documented with few analyses performed on rocks erupted prior to 1960. However, there are indications that the early Anak Krakatau lavas did not differ significantly in composition from more recent eruptives, as silica content in ashes and bombs erupted in the period 1928–1935 have been reported to be in the range of 51.81–54.76 wt% (van Bemmelen 1949), overlapping with the SiO<sub>2</sub> content of the recent basaltic andesites (Fig. 3).

This corresponds well with the observation of Camus et al. (1987) that the composition of the tuff ring and lava flows on Anak Krakatau appeared to belong invariably to the basaltic andesite suite. Field observations by the two lead authors in 2008 also supports this, as the lava bombs of the 2007–2008 eruptions appear to be virtually identical petrographically to the 2002 bombs described by Gardner et al. (2006, *in press*). Thus, all whole rock analyses and field observations are consistent with the conclusion that the bulk of Anak Krakatau is made up of basaltic andesite, with minor components of basalt plus sparse acidic-andesite.

### Previous estimates of magma storage depth

Estimates and constraints of magma storage beneath the Krakatau complex have been previously derived using (a) plagioclase-melt thermobarometry, (b) chlorine content in melt inclusions, (c) loci of seismic attenuation zones and (d) in situ crystal isotope stratigraphy.

Mandeville et al. (1996a) employed plagioclase-melt thermobarometry (after Housh and Luhr 1991) and chlorine content in melt inclusions (after Metrich and Rutherford 1992) to estimate the depth of the 1883 magma chamber. Their results indicate shallow depths of magma storage, with pressure estimates in the range of 100–200 MPa (~4 to 8 km) for plagioclase crystallization, and ca. 100 MPa (~4 km) derived from chlorine inclusions. Camus et al. (1987) used plagioclase-melt thermobarometry (after Kudo and Weill 1970) to estimate pressures of crystallization for

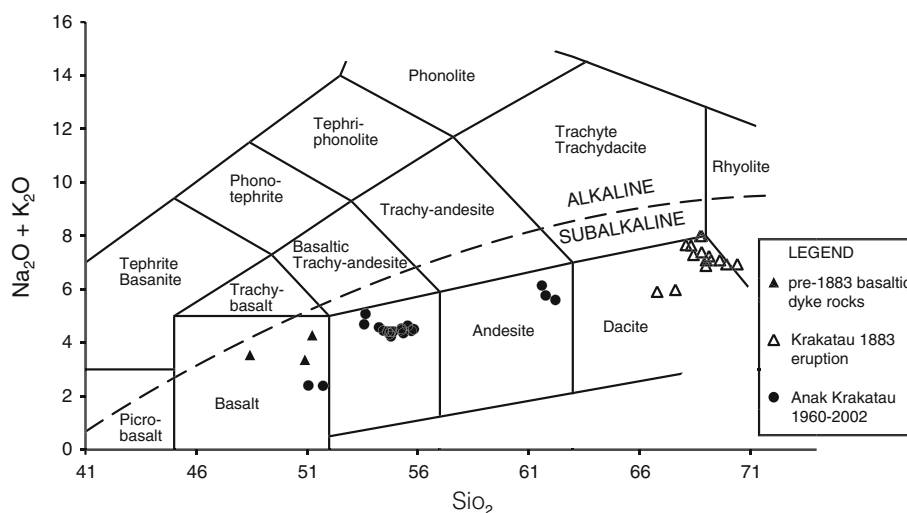


**Fig. 3** Total alkalis versus silica (TAS) diagram (Le Bas et al. 1986) plotting bulk composition of rocks from Anak Krakatau (circles) and Krakatau (triangles) (data from Zen and Hadikusumo 1964; Self 1982; Camus et al. 1987; Mandeville et al. 1996a; Gardner et al. *in press*). The Krakatau rocks include products from the 1883 rhyodacite

eruption (open triangles) as well as older basaltic dyke rocks (filled triangles). The vast majority of the rocks erupted from Anak Krakatau plot in a very narrow range in the basaltic andesite field, with single eruptive events only in the basalt and andesite fields

plagioclase in rocks erupted in 1883 (Krakatau) and between 1973 and 1981 (Anak Krakatau), arriving at an estimate of 50–200 MPa ( $\sim 2$  to 8 km) for both Krakatau and Anak Krakatau lavas. Gardner et al. (2006, *in press*) carried out *in situ*  $^{87}\text{Sr}/^{86}\text{Sr}$  analyses employing LA-ICPMS on plagioclase from the 2002 eruptions of Anak Krakatau. This work illustrates that late crystallization of many plagioclase grains must have taken place during assimilation of sedimentary country rock. This observation constrains the depth of late stage plagioclase crystallization, on simple stratigraphic grounds (Fig. 2a), to within the upper 3–6 km (Nishimura and Harjono 1992; Lelgemann et al. 2000), which is in good agreement with the plagioclase-melt thermobarometry results discussed above.

Harjono et al. (1989) analysed the seismic signature from 14 earthquakes near Anak Krakatau in 1984, using data from analogue seismograms. Two seismic attenuation zones beneath the volcanic edifice were identified in that study: one a small and irregular zone at a depth of approximately 9 km and another much larger area at 22 km (Fig. 2b). These were thought to represent the granite-diorite/gabbro transition and the Moho, respectively (Fig. 2a). However, a lack of data from the lower crust meant that it was not possible to decide whether or not these two attenuation zones are connected. It also remains unresolved if these two zones represent large-volume chambers or a concentration of smaller melt pockets, which is relevant for estimating long-term magma storage volumes and hence the availability of magma for eruption. Harjono et al. (1989) did, however, speculate that the mid-crustal storage region (9 km) is made up of separate magma pockets with a combined volume large enough to differentiate an eruptive volume in the order of 10–15 km<sup>3</sup>, i.e. comparable to the volume erupted in the caldera-forming eruption of 1883. The deep storage region (22 km), on the other hand, was thought to be considerably larger, both in terms of volume and extension (Fig. 2b, Harjono et al. 1989).

In summary, petrological studies have previously identified shallow magma storage in the region of 2–8 km beneath Krakatau (Camus et al. 1987; Mandeville et al. 1996a; Gardner et al. 2006, *in press*), whereas seismic evidence points towards mid- to deep-crustal storage zone(s), at 9 and 22 km, respectively (Harjono et al. 1989). This discrepancy between the results is likely due to inherent limitations in both methods. Seismic studies cannot resolve small-volume magma bodies and petrological methods are dependent on mineral phases and melt inclusions retaining a complete record of pressure, temperature and compositional parameters that have changed during the various stages of magma ascent and evolution.

## Methods

### EMP analytical procedure

Mineral chemistry as well as glass and groundmass compositions from basaltic andesites erupted in the period 1990–2002 was analysed at two different EMP facilities: a Cameca SX 50 at Uppsala University (Sweden) and a JEOL JXA-8200 Superprobe at Copenhagen University (Denmark). For the Cameca EMP, an accelerating voltage of 20 kV and a current of 15 nA was used, while the JEOL EMP was calibrated using an accelerating voltage of 15 kV and a current of 15 nA. The beam diameter was generally 1–2  $\mu\text{m}$ , though a defocused spot was used for the analysis of groundmass and glass composition. These ‘defocused spot’ analyses of groundmass included glass and microcrysts, but avoided phenocrysts. Glass compositions were not only analysed from the groundmass but also in melt inclusions. International reference materials were used for calibration and standardization (e.g. Andersson 1997). For elements with abundances greater than 1 wt%, the reproducibility is  $<\pm 10\%$ , while for abundances less than 1 wt%, the reproducibility is  $>\pm 10\%$ .

The analysed data set consists of 297 clinopyroxene, 375 plagioclase, 39 olivine and 92 orthopyroxene spot analyses, collected from 63 clinopyroxene, 71 plagioclase, 11 olivine and 36 orthopyroxene distinct crystals. Also, 14 analyses of glass in groundmass and melt inclusions were collected as well as another 14 defocused spot ( $\sim 10 \times 10 \mu\text{m}$ ) analyses of groundmass, in order to calculate an average groundmass composition that includes both glass and microcrystalline phases. All analytical data are reported in the electronic appendix.

### Clinopyroxene-melt thermobarometers

Two models based on clinopyroxene-melt equilibria have been applied. The first thermobarometer is based on the jadeite-diopside/hedenbergite exchange equilibria between clinopyroxene and coexisting melt (Putirka et al. 2003). This model has proved to be able to recreate  $P$ – $T$  conditions for a wide range of magma compositions, within a reasonable margin of error, and has been frequently used in the last decade (e.g. Shaw and Klügel 2002; Putirka and Condit 2003; Schwarz et al. 2004; Caprarelli and Riedel 2005; Klügel et al. 2005; Galipp et al. 2006; Mordick and Glazner 2006; Longpré et al. 2008; Barker et al. 2009). Crucially, it has proved to be applicable to analogue (high  $P$ – $T$ ) experiments (Putirka 2008) while also correlating well with independent methods for natural samples (Klügel and Klein 2005). The Putirka et al. (2003) thermobarometer will henceforth be termed PTB03. The standard errors

of estimate (SEE) for PTB03 are  $\pm 33^\circ\text{C}$  and  $\pm 170$  MPa (Putirka et al. 2003).

The second clinopyroxene-melt model to be used for comparison is a barometer based on the Al partitioning between melt and clinopyroxene, calibrated especially for hydrous systems, requiring the input of a specific  $\text{H}_2\text{O}$  concentration (Putirka 2008, eqn. 32c). This model will be referred to as PB08. The PB08 formulation also requires the input of a temperature value, which can be provided by the PTB03 model. Note that PB08 is not as firmly tested as PTB03, but the SEE of  $\pm 150$  MPa is thought to be superior to that of PTB03 (Putirka 2008).

As PTB03 and PB08 are based on independent clinopyroxene-melt exchange equilibria (Na and Al, respectively), these models are used in conjunction to provide an internal validation of results.

#### Clinopyroxene composition barometer

To test the results of the Putirka clinopyroxene-melt thermobarometry (PTB03 and PB08), a clinopyroxene barometer not requiring the input of a coexisting melt can be used. The clinopyroxene composition barometer developed by Nimis (1995, 1999) and Nimis and Ulmer (1998) is widely used, despite a reported tendency of systematically underestimating pressures when applied to hydrous systems (Putirka 2008). To eliminate this systematic error, this barometer was re-calibrated for hydrous systems by Putirka (2008, eqn. 32b), with the added requirement of an  $\text{H}_2\text{O}$  estimate in addition to the temperature estimate already needed. This barometer will be referred to as NimCal08. The SEE for NimCal08 is estimated to  $\pm 260$  MPa (Putirka 2008).

#### Plagioclase-melt thermobarometer

Since the first plagioclase thermometer was formulated (Kudo and Weill 1970), the approach has been developed further by various workers including geobarometers (Housh and Luhr 1991; Sugawara 2001; Ghiorso et al. 2002; Putirka 2005, 2008). Putirka (2005, 2008) calibrated the plagioclase-melt thermobarometer for hydrous systems, requiring the input of a  $\text{H}_2\text{O}$  estimate in the modelling calculations. However, the uncertainty in plagioclase-melt geobarometry remains significant and, occasionally and apparently randomly, produces very poor results from some data sets (Putirka 2008). The SEE for the plagioclase-melt thermobarometer is  $\pm 36^\circ\text{C}$  and  $\pm 247$  MPa (Putirka 2008).

#### Olivine-melt thermometer

The Putirka et al. (2007) olivine-melt thermometer, specifically calibrated for hydrous systems, will be used in this

study. The SEE of this olivine-melt thermometer is  $\pm 29^\circ\text{C}$  (Putirka 2008).

We have employed this thermometer to provide an independent test for the reliability of our clinopyroxene-melt thermobarometry. As olivine is assumed to have formed prior to and/or together with clinopyroxene, calculated olivine crystallization temperatures are expected to overlap or be slightly higher than calculated clinopyroxene temperatures. Such a match would indicate reliable results (e.g. Longpré et al. 2008).

#### Seismic tomography

The seismic structure beneath the Krakatau complex and surrounding areas has been studied using local earthquake tomographic inversion (Hoffmann-Rothe et al. 2006; Jaxybulatov et al. 2011). The data for this study were collected within the seismological part of the KRAKMON Project (Hoffmann-Rothe et al. 2006; Ibs-von Seht 2008). Fourteen temporary seismic stations were installed on the islands of the Krakatau archipelago and in surrounding areas of the Sunda Strait, Sumatra and Java. The survey was conducted between June 2005 and January 2006. The data set used in this study includes more than 700 local events with arrival times of 3128 P- and 2050 S-phases. The data processing is based on the LOTOS code (Koulakov 2009), which is used for the nonlinear tomographic inversion of P and S arrival times to the distributions of P and S velocities, as well as  $V_p/V_s$  ratio and source locations. The resolution limitations due to unfavourable configuration of the network were thoroughly investigated in Jaxybulatov et al. (2011) using a series of different synthetic tests.

#### Input parameters

##### Mineral-melt equilibrium tests

Finding the appropriate equilibrium melt compositions for mineral-melt thermobarometric models is of key importance for accurate results. This is the single largest source of error in mineral-melt equilibria models, which means that rigorous evaluation of any nominal melt of choice for equilibrium is critically important. Equilibrium tests are commonly performed using exchange coefficients of elements between mineral and melt (e.g. Klügel and Klein 2005; Longpré et al. 2008; Barker et al. 2009). For clinopyroxene and olivine, the equilibrium exchange coefficients for iron and magnesium ( $K_{d[\text{FeMg}]}$ ) are expected to be  $0.28 \pm 0.08$  and  $0.30 \pm 0.03$ , respectively (Roeder and Emslie 1970; Duke 1976; Putirka 2008). Mineral-melt pairs with  $K_{d[\text{FeMg}]}$  values falling outside these boundaries should be discarded.

For clinopyroxene, it is also useful to consider the equilibrium partitioning of other components such as Na–Ca–Al (Rhodes et al. 1979; Putirka 1999, 2008). The equilibrium test suggested by Putirka (1999) predicts the relative amounts of different clinopyroxene mineral components that would crystallize from a given equilibrium melt at the estimated  $P$ – $T$  conditions. The “predicted mineral components” (PMC) can then be compared with the “observed mineral components” (OMC). A close match would support equilibrium conditions.

The recommended equilibrium test for plagioclase–melt thermobarometry uses the ratio of the partitioning coefficients of the anorthite and albite components,  $Kd_{[An-Ab]}$  (Putirka 2005, 2008). This is expected to be  $0.10 \pm 0.05$  at  $T < 1,050^\circ\text{C}$  and  $0.27 \pm 0.11$  at  $T > 1,050^\circ\text{C}$  (Putirka 2008). Only the plagioclase datapoints closest to equilibrium with the selected nominal melt should be considered reliable. As a further test for equilibrium, the temperature estimate will be compared with a plagioclase saturation surface temperature calculated for the nominal melt, with a SEE of  $\pm 37^\circ\text{C}$  (Putirka 2008, eqn. 26). The plagioclase saturation surface temperature is the lowest possible temperature for the nominal melt, at a given pressure, before plagioclase starts crystallizing. A close match between the temperature estimates of the plagioclase–melt and plagioclase saturation thermometers is expected for close to perfect equilibrium conditions (Putirka 2008).

#### Pre-eruptive $\text{H}_2\text{O}$ content

The  $\text{H}_2\text{O}$  content is a very influential parameter in a number of the thermobarometers that are used in this study. The pre-eruptive volatile content of a rock can be approximated from the mass deficiency in EMP analyses of groundmass glass and melt inclusions (‘the difference method’), as described in Devine et al. (1995), provided that the volatiles make up  $>1\%$ . Anak Krakatau melt inclusions represent the melt composition of the magma during different stages of its evolution prior to degassing and eruption. The mass deficiency in the glass inclusions measured here ranges from 1.2 to 4.9 wt% (average = 2.4 wt%;  $n = 9$ ). However, the precision of the ‘difference method’ is not very high (generally around  $\pm 0.5\%$ ; Devine et al. 1995). Mandeville et al. (1996a), also using the ‘difference method’, estimated the pre-eruptive volatile content in 1883 Krakatau rhyolites and dacites to be  $4 \pm 0.5$  wt%. Basalts and basaltic andesites should be  $\text{H}_2\text{O}$  saturated at a lower  $\text{H}_2\text{O}$  content than is the case for more evolved compositions, leading to the assumption that melt inclusions with low volatile content likely represents melt captured at an earlier stage of magma evolution. Therefore, we will use a range of values from 2 to 4 wt%  $\text{H}_2\text{O}$  for the thermobarometric calculations to follow. The higher end of

that range (3–4 wt%) will be considered for basaltic andesite whole rock compositions, while the lower end (2–3 wt%) will be considered for basaltic compositions.

#### Bedrock density

For the conversion of pressure estimates (MPa) to depth (km), the approximate densities of the respective stratigraphic units below Krakatau have been estimated. In the study by Kopp et al. (2001), a seismic line over the Java trench was investigated, ending just  $\sim 10$  km south of Krakatau. The stratigraphy proposed in that study will be used here as the basis for estimating the densities of bedrock units beneath Anak Krakatau (Table 1).

## Results

### Petrography and mineral chemistry

The basaltic andesite lavas examined are all highly porphyritic (30–35%), dark in appearance, and in part vesicular. Plutonic as well as sedimentary xenoliths occur. The homogeneity of the whole rock chemistry is reflected in the petrographic features. All thin sections examined share the same characteristics, as well as a relatively homogenous mineral chemistry, especially with respect to clinopyroxene. In order of relative abundance, the mineral phases in the rocks are plagioclase  $>$  clinopyroxene  $>$  orthopyroxene  $>$  titanomagnetite  $>$  olivine. The modal composition is on average, 70% groundmass, 25% plagioclase, 4% clinopyroxene and less than 1% olivine phenocrysts or micro-phenocrysts (cf. Camus et al. 1987; Gardner et al. *in press*). These phenocryst phases will be described below. Selected microphotographs and electron backscatter images are displayed in Fig. 4. Representative compositions of plagioclase, clinopyroxene and olivine are reported in Table 2. All EMP analyses are available as an electronic appendix.

### Plagioclase

Plagioclase phenocrysts are mostly subhedral, but a few are anhedral. Sieve-like textures are a common feature with numerous melt inclusions present. The size of the plagioclase crystals is on the order of 0.5–2 mm. Many plagioclase crystals, when viewed under polarized light, appear to have experienced stages of growth, dissolution and overgrowth. Some cores are rounded and appear partially resorbed. Such cores are often surrounded by sieve-like (or cellular) zones ending with a thin rim (e.g. Fig. 4a, c). Other crystals lack resorbed cores, but carry numerous melt inclusions (Fig. 4b). Normal, complex and reverse zoning

**Table 1** Estimated densities of crustal rocks below Anak Krakatau

Inferred rock types	Depth (km) (Harjono et al. 1989)	Density (g cm <sup>-3</sup> ) (Kopp et al. 2001)
Sedimentary succession	0–4	2.32 (2.23–2.4)
Granitoids	4–9	2.8
Diorite/gabbro	9–22	2.95
Mantle	>22	3.37

**Table 2** Representative mineral compositions from Anak Krakatau eruptives

Mineral	plag	plag	plag	plag	plag	cpx	cpx	Ol
Notes	Core, An <sub>90</sub>	Rim, An <sub>79</sub>	Rim, An <sub>66</sub>	Rim, An <sub>51</sub>	Core, An <sub>45</sub>	Mg# = 0.61	Mg# = 0.63	Core, Fo <sub>72</sub>
Analysis no:	kcs24plag44a	4_AKXCI 11 tr2 11	3_AK1 1 fsp p13	4_AKXCI 11 tr3 63	4_AKXCI 11 tr3 11	cpx 6	cpx 11	3_AKXIC 04 p35
SiO <sub>2</sub>	45.06	48.22	50.94	55.54	57.05	51.62	51.38	37.08
TiO <sub>2</sub>	0.027	0.00	0.057	0.04	0.01	0.69	0.64	0.02
Al <sub>2</sub> O <sub>3</sub>	34.47	31.95	30.06	27.06	25.77	2.23	2.26	–
FeOt	0.527	0.70	0.74	0.54	0.48	9.77	9.17	25.23
MnO	0.024	–	–	–	–	0.35	0.33	0.42
MgO	0.087	–	–	–	–	15.34	15.63	36.73
CaO	18.16	16.13	13.90	10.85	9.73	19.80	19.86	0.21
Na <sub>2</sub> O	1.046	2.28	3.84	5.49	6.31	0.20	0.19	–
K <sub>2</sub> O	0.028	0.06	0.09	0.17	0.20	–	–	–
Cr <sub>2</sub> O <sub>3</sub>	0.015	–	–	–	–	0.01	0.01	–
Total	99.44	99.34	99.63	99.69	99.55	100.0	99.47	99.69

have been documented. This is illustrated by the fact the lowest anorthite concentrations (An<sub>45</sub>) as well as the highest (An<sub>90</sub>) were found in plagioclase cores, though the majority of the low-An composition was found in the rims, and the highest An contents (~An<sub>80–90</sub>) were only found in the cores. Similarly, the rims also vary widely in their compositional range, between An<sub>79</sub> and An<sub>50</sub>. However, plagioclase compositions in the range of ~An<sub>60–70</sub> are typically found in sieve-like zones, rims and groundmass microcrysts, implying that this composition is closest to equilibrium with the host rock. The composition of all plagioclase datapoints analysed for this study is illustrated in Fig. 5a, b.

### Clinopyroxene

The clinopyroxene crystals are, with few exceptions, euhedral. Most grains have melt inclusions, though considerably fewer than in plagioclase. The clinopyroxene crystals are slightly smaller than plagioclase, in the region of 0.2–1.0 mm. Also, it is common to find plagioclase that has grown around clinopyroxene, implying that plagioclase growth occurred largely after clinopyroxene crystallization (Fig. 4d). The two mineral phases may thus record different stages of magma storage and crystallization. For reference,

compositional data of clinopyroxenes from Mandeville et al. (1996a) and Camus et al. (1987) have been included as a subset in the model calculations. The mineral chemistry of clinopyroxene is very homogenous with very little variation within individual grains. Therefore, in the case of clinopyroxene, the average composition of each individual grain was calculated and used in the thermobarometric calculations.

Following Morimoto et al. (1988), the compositions of pyroxene are plotted in Fig. 5c. All the analysed clinopyroxenes belong to the same compositional family. Core-rim variations are minor, with a tendency for normal zoning towards slightly more Fe-rich rims, but the opposite has also been observed in some grains. The recent (1990–2002) and old (1883–1981) clinopyroxenes are compositionally similar, despite occurring in basaltic andesite, andesite and even rhyodacite host rocks, and erupted over >100 years (i.e. 1883 and 2002).

### Olivine

Olivine is a relatively rare phase in our analysed samples (<1%) and has not been identified in all thin sections. The olivines present are small, with diameters in the order of 0.02–0.15 mm, and are best identified using electron backscatter images and EMP analyses. All olivines

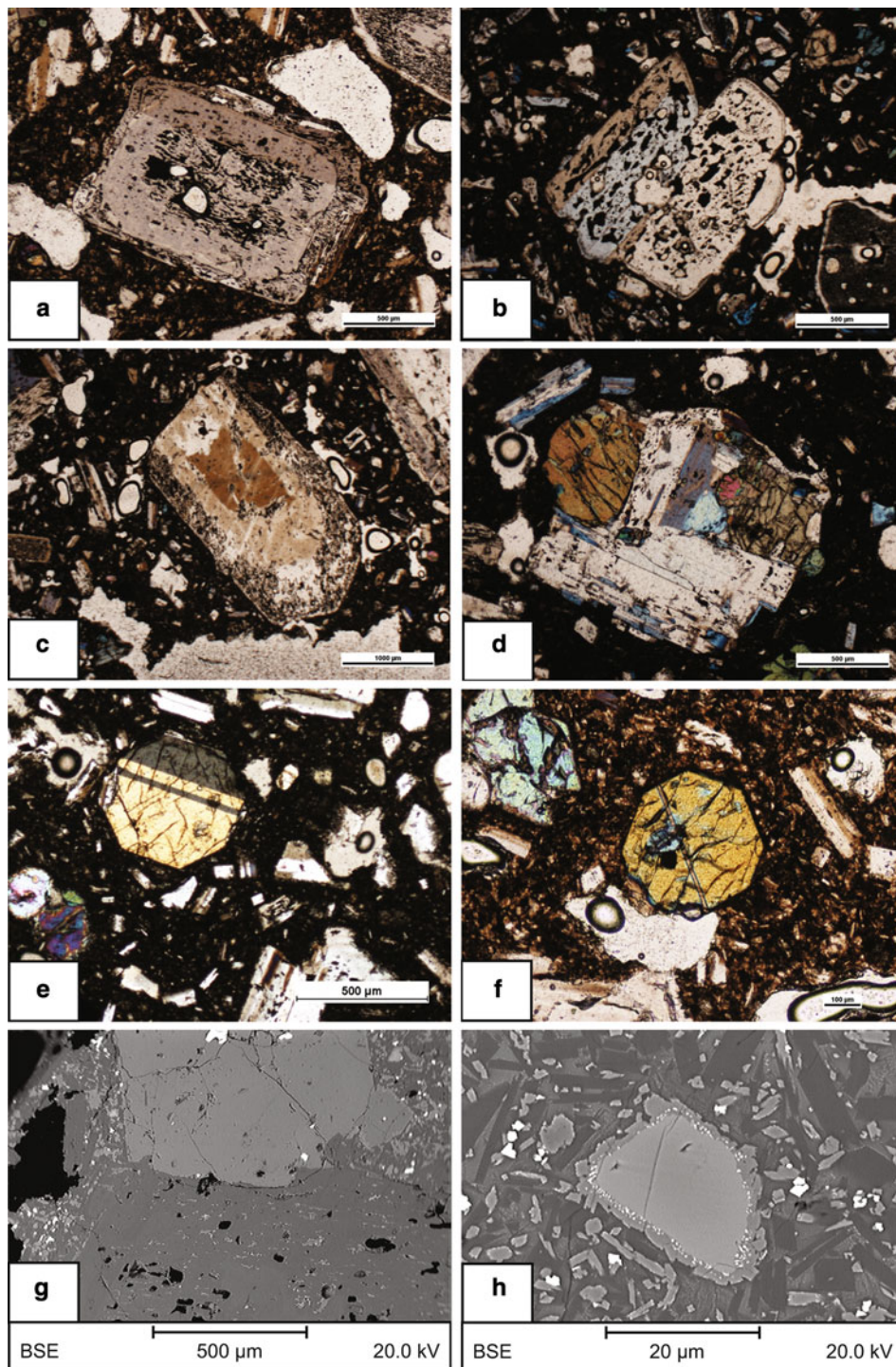


**Fig. 4** Representative microphotographs (*crossed polars*) and BSE images of **a** subhedral plagioclase crystal with highly sieve-textured core and rim regions, reflecting a dynamic magma system. **b** Sieve-textured plagioclase crystal with numerous melt inclusions. Note also the very thin overgrowth rim. **c** Plagioclase crystal with resorbed core. The outer regions are sieve-textured with a thin overgrowth on the rims (cf. Fig. 4a, b). **d** A plagioclase crystal intergrown with several smaller clinopyroxene crystals. **e** Euhedral, twinned clinopyroxene crystal. In the *bottom left corner*, there is a small, partly resorbed olivine with very high interference colours. Note that the olivine has a

discontinuous reaction rim with orthopyroxene and titanomagnetite, as can also be seen in **h** below. **f** Euhedral clinopyroxene crystal. *Dark brown*, vesicular groundmass consisting of acicular plagioclase, orthopyroxene, titanomagnetite and glass. **g** BSE image of intergrown plagioclase (*bottom*) and clinopyroxene (*top*). **h** BSE image of a partly resorbed olivine (*centre of image*), covered by discontinuous overgrowth of orthopyroxene and titanomagnetite. The olivine crystal is surrounded by acicular plagioclase (*dark grey laths*), anhedral orthopyroxene (*light grey*), titanomagnetite (*white crystals*) and glass (*irregular dark grey fields*)

observed are anhedral (resorbed), frequently with rims covered by overgrowth of orthopyroxene and occasional titanomagnetite (Fig. 4h). There is a gradual normal zoning in all the olivine crystals investigated with generally more Fe-rich rims. Forsterite content ranges between Fo<sub>63–80</sub>, with most olivine rims falling below Fo<sub>70</sub>.

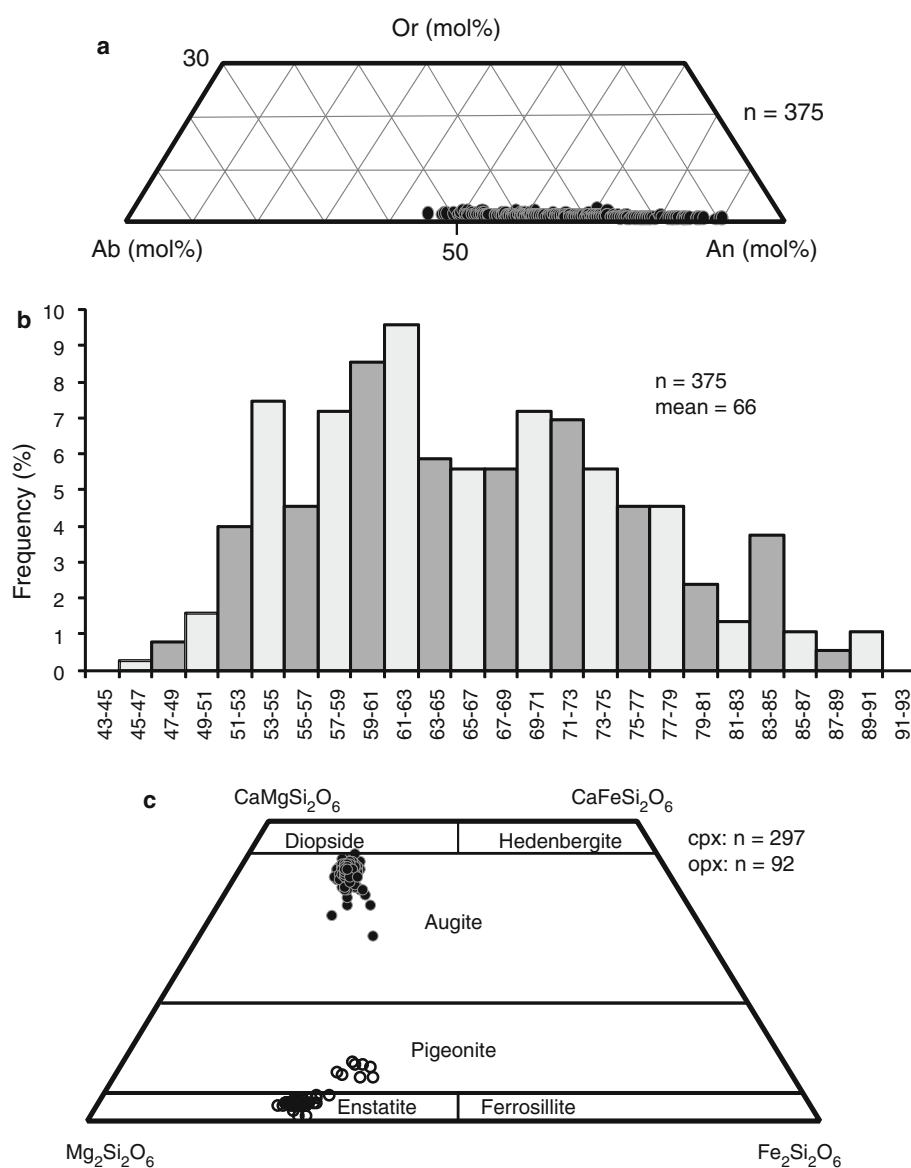
#### Pressures and temperatures from clinopyroxene-melt thermobarometry

The clinopyroxenes exhibit no clear petrographic indicators of being out of equilibrium with the host melt, as they are commonly euhedral and lack strong compositional zoning. However, euhedral habit and the lack of zoning does not by itself verify equilibrium between clinopyroxene and host melt, especially considering the sluggishness

of clinopyroxene re-equilibration, which is on the order of months to years for a 5–10  $\mu\text{m}$  rim (Cashman 1990). The rather short repose time at Anak Krakatau volcano, often with a dozen eruptive pulses during a single year (Siebert and Simkin 2002), is unlikely to allow sufficient time for full re-equilibration during shallow residence of the magma.

The most commonly used nominal melts are whole rock, groundmass and glass compositions (e.g. Shaw and Klügel 2002; Putirka and Condit 2003; Putirka et al. 2003; Caprarelli and Riedel 2005; Klügel et al. 2005; Longpré et al. 2008). In addition to these, a more primitive whole rock from an Anak Krakatau lava flow from the eruptive period 1960–1963 (henceforth labelled 1963 basalt) will be evaluated here (Zen and Hadikusumo 1964). In Fig. 6a, the  $Kd_{[\text{FeMg}]}$  of the four nominal melt options are compared.

**Fig. 5** **a** Composition of all analysed plagioclase datapoints ( $n = 375$ ). Plagioclase composition varies between An<sub>45</sub> and An<sub>90</sub>. **b** Histogram of all analysed plagioclase. **c** Composition of clinopyroxene (filled circles,  $n = 312$ ) and orthopyroxene (open circles,  $n = 92$ ) crystals. The clinopyroxene data set includes compositions of minerals analysed for this study ( $n = 297$ ) and data from the literature ( $n = 15$ ; Camus et al. 1987; Mandeville et al. 1996a). All clinopyroxene data plots in a narrow region in the augite field. The compositions of the orthopyroxene crystals are slightly more heterogeneous, spreading over the enstatite and pigeonite fields



Only the 2002 basaltic andesite and the 1963 basalt plot within the  $Kd_{[FeMg]} = 0.28 \pm 0.08$  interval and can thus be assumed to represent liquids in potential equilibrium with the analysed clinopyroxenes (cf. Putirka 2008).

In Fig. 6b, the observed and predicted Diopside-Hedenbergite (DiHd) components are plotted, using (a) the 1963 basalt and (b) the 2002 basaltic andesite composition. Both compositions result in virtually identical distributions, with 77% of the datapoints plotting within 5% of the theoretical equilibrium. It is not possible, using only these methods, to determine whether the 1963 basalt or 2002 basaltic andesite is more appropriate as the equilibrium melt. However, using the 2002 basaltic andesite, as much as 78% of the datapoints result in negative pressures (range =  $-1,296$  to  $187$  MPa, average =  $-203$  MPa). Therefore, the 2002 basaltic andesite is a less viable nominal melt, despite successfully passing the equilibrium tests. The 1963 basalt, producing more realistic pressures, is therefore taken as the most reliable nominal melt option to use in our calculations, i.e. the clinopyroxenes crystallized from a basaltic magma. All mineral-melt pairs that fall out of the equilibrium range in the DiHd test are ignored for the  $P$ - $T$  calculations.

The three sets of calculated clinopyroxene crystallization pressures using the 1963 basalt as nominal melt range from  $59$  to  $377$  MPa, with a high degree of overlap between the results from PTB03 and PB08 (Fig. 7). The PTB03 and PB08 models were also applied to published clinopyroxene compositions (Camus et al. 1987; Mandeville et al. 1996a), erupted between 1883 and 1981 (also using the 1963 basalt composition as nominal melt). These older clinopyroxenes were also subjected to the array of equilibrium tests described above (Fig. 6). The recorded  $P$ - $T$  conditions of these older clinopyroxenes spread over a much larger interval of calculated pressures ( $116$ - $759$  MPa), broadly in agreement with the results obtained for clinopyroxenes analysed in this study. Generally, the older clinopyroxenes record slightly higher pressures and temperatures as compared to those obtained for lavas erupted between 1990 and 2002 (Fig. 7c). This potentially indicates that clinopyroxenes in lavas erupted prior to 1981 crystallized at a greater depth than the more recently erupted clinopyroxenes, pointing towards a shallowing of the magma system over the last 30 years. However, this remains somewhat speculative, and further testing is required to substantiate a long-term pattern. All results of PTB03 and PB08 are reported in Table 3.

#### Pressure estimates from clinopyroxene barometry

The NimCal08 barometer (Putirka 2008, eqn. 32b), making use of temperature estimates calculated through the PTB03 model, yields pressures slightly lower than the PTB03 and

PB08 models, but with a significant overlap (Table 3; Fig. 7b, d). Estimates of  $2H_2O$  and  $3H_2O$  result in average pressures of  $103$  MPa ( $-57$  to  $214$ ) and  $148$  MPa ( $-11$  to  $259$ ), respectively. As mentioned above, this model is not deemed particularly precise nor accurate, with a tendency for systematically underestimating crystallization pressures (Putirka 2008). However, the overall overlap with model results from PTB03 and PB08 lends credence to the calculations. For a comparison of the results of PTB03, PB08 and NimCal08 models, see Fig. 7d.

#### Pressures and temperatures from plagioclase-melt thermobarometry

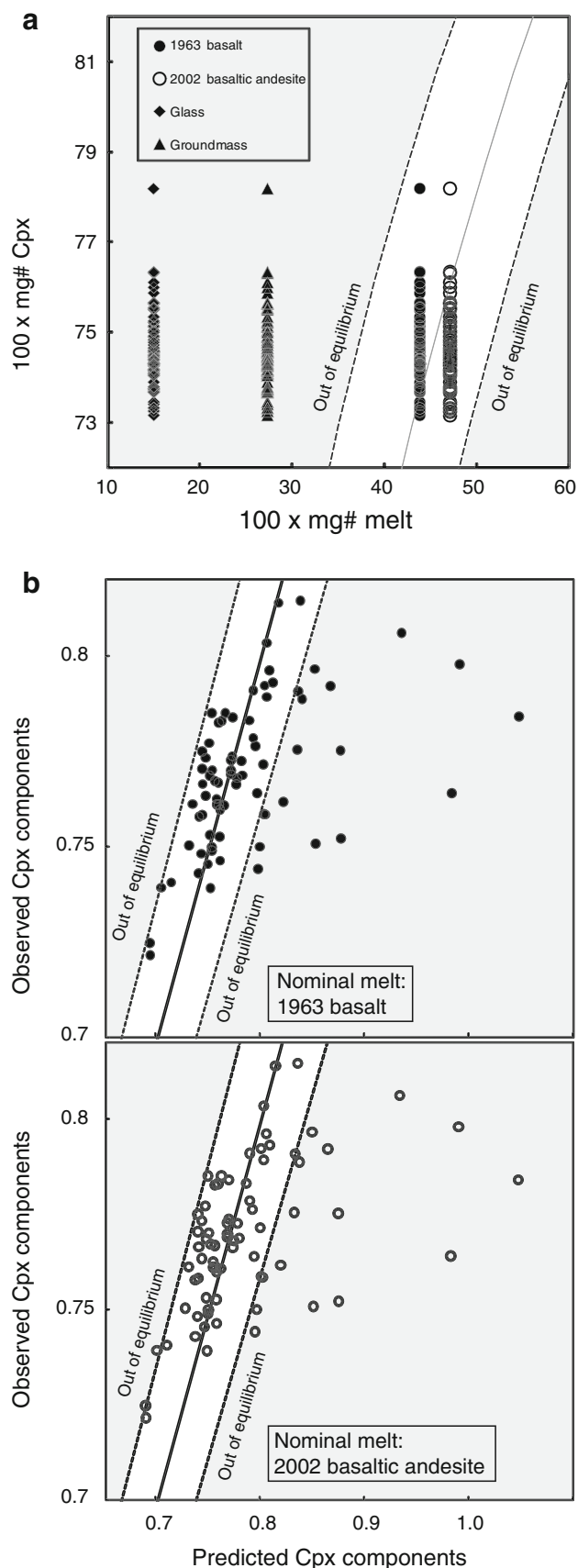
The  $Kd_{[Ab-An]}$  equilibrium test (Fig. 8a) indicates that plagioclase in the compositional range of  $An_{56-76}$  (68% of analysed datapoints) is in equilibrium with the 2002 basaltic andesite, whereas the high-anorthite plagioclase ( $An_{77-88}$ , 11% of analysed datapoints) are closer to equilibrium with the 1963 basalt. The low-An compositional range ( $An_{45-56}$ , 21% of analysed datapoints) is out of equilibrium with all tested nominal melts, and these compositions are not considered for the model calculations. The medium anorthite compositions ( $An_{56-76}$ ) that are in equilibrium with the whole rock are commonly found in sieve-like zones, rims and groundmass microcrysts, providing a textural indication that this compositional range should be closest to equilibrium with the host rock. Furthermore, using an input of  $>3.5$  wt%  $H_2O$ , the temperature estimates calculated are invariably below  $1,050^\circ C$ , requiring a different set of  $Kd_{[Ab-An]}$  equilibrium conditions (Putirka 2008). This means that the plagioclase is not in equilibrium with the whole rock at  $>3.5$  wt%  $H_2O$ , effectively constraining pre-eruptive  $H_2O$  content in the recent basaltic andesites to  $\leq 3.5$  wt%  $H_2O$ . A further indication of the suitability of the selected nominal melts for plagioclase-melt thermobarometry is the fact that the plagioclase saturation surface temperatures calculated are only  $3$ - $15^\circ C$  higher than the temperature estimated using the plagioclase-melt thermometer, which is well within the SEE for the plagioclase saturation model of  $\pm 37^\circ C$  (Putirka 2008). There is a strong correlation between  $Kd_{[Ab-An]}$  and the  $P$ - $T$  estimates. The highest and lowest  $P$ - $T$  estimates correlate with the  $Kd_{[Ab-An]}$  farthest removed from the ideal value of  $0.27$ . Therefore, the average  $P$ - $T$  estimate for each data set  $\pm 1\sigma$  will be considered, as this removes the less reliable results. Looking exclusively at these "best fit" plagioclases, two very tight ranges of  $P$ - $T$  estimates are derived (Table 4; Fig. 8b). The plagioclase in equilibrium with the 2002 basaltic andesite ( $An_{56-76}$ ) records pressures between  $23$  and  $186$  MPa. The high-anorthite plagioclase ( $An_{77-88}$ ) in equilibrium with the 1963 basalt, in contrast, records pressures between  $645$  and

**Fig. 6 a** Test for equilibrium using the  $K_{d[FeMg]}$  between clinopyroxene and melt. The 1963 basalt and 2002 basaltic andesite both result in  $K_{d[FeMg]}$  values close to the ideal of 0.28 (Putirka 2008). They have therefore been selected as the melt compositions with which the clinopyroxenes are most likely to have equilibrated. **b** The predicted versus observed mineral components of diopside + hedenbergite, derived using the two nominal equilibrium melts 1963 basalt (top) and 2002 basaltic andesite (bottom). Both nominal melts give very similar results, in terms of predicted mineral compositions, indicating that both need to be considered viable as potential equilibrium melts

807 MPa. In other words, these high-anorthite plagioclase compositions formed in a deeper storage region, after which the magma was transported to shallower levels where crystallization of more albitic plagioclase took place. Calculated plagioclase and clinopyroxene crystallization depths are compared in Fig. 10 and Table 6.

Temperature estimates from olivine-melt thermometry

Due to the petrological evidence of resorption, olivine is not considered a stable phase in the basaltic andesite host rock. Thus, neither the 2002 basaltic andesite whole rock nor its groundmass compositions can be considered feasible equilibrium melts for olivine-melt thermometry. However, the olivine present is likely to have crystallized in equilibrium with a more primitive melt, similar in composition to the 1963 basalt lava. The  $K_{d[FeMg]}$  values for olivine and the 1963 basalt whole rock composition (Zen and Hadikusumo 1964) were compared with the equilibrium  $K_{d[FeMg]}$  value ( $0.30 \pm 0.03$ ) of Roeder and Emslie (1970). The 1963 basalt fulfils the equilibrium requirements with olivine in the very narrow compositional range of Fo<sub>70–72</sub>, representing only 28% of all analysed olivine datapoints (Fig. 9a). Using the 1963 basalt and H<sub>2</sub>O contents of 2 and 3 wt%, the olivine-melt thermometry results in a range of temperatures from 1,124 to 1,145°C (see Table 5). The results, and a comparison with the calculated clinopyroxene and plagioclase crystallization temperatures, are plotted in Fig. 9b. The temperatures estimated for olivine overlap with the temperatures estimated for clinopyroxene as well as for high-anorthite plagioclase—all of which appear to be in equilibrium with the 1963 basalt. Meanwhile, the medium-anorthite plagioclase (An<sub>56–76</sub>) in equilibrium with the 2002 basaltic andesite forms a distinct cluster of lower temperatures. Note also that the calculated olivine temperatures are marginally higher than for clinopyroxene and high-anorthite plagioclase, which would fit well with the modelling of liquid line of descent from Putirka et al. (2007), suggesting that olivine would be the first phase to precipitate from this type of liquid. Crucially, the fact that the olivine-melt, clinopyroxene-melt and plagioclase-melt thermometers are



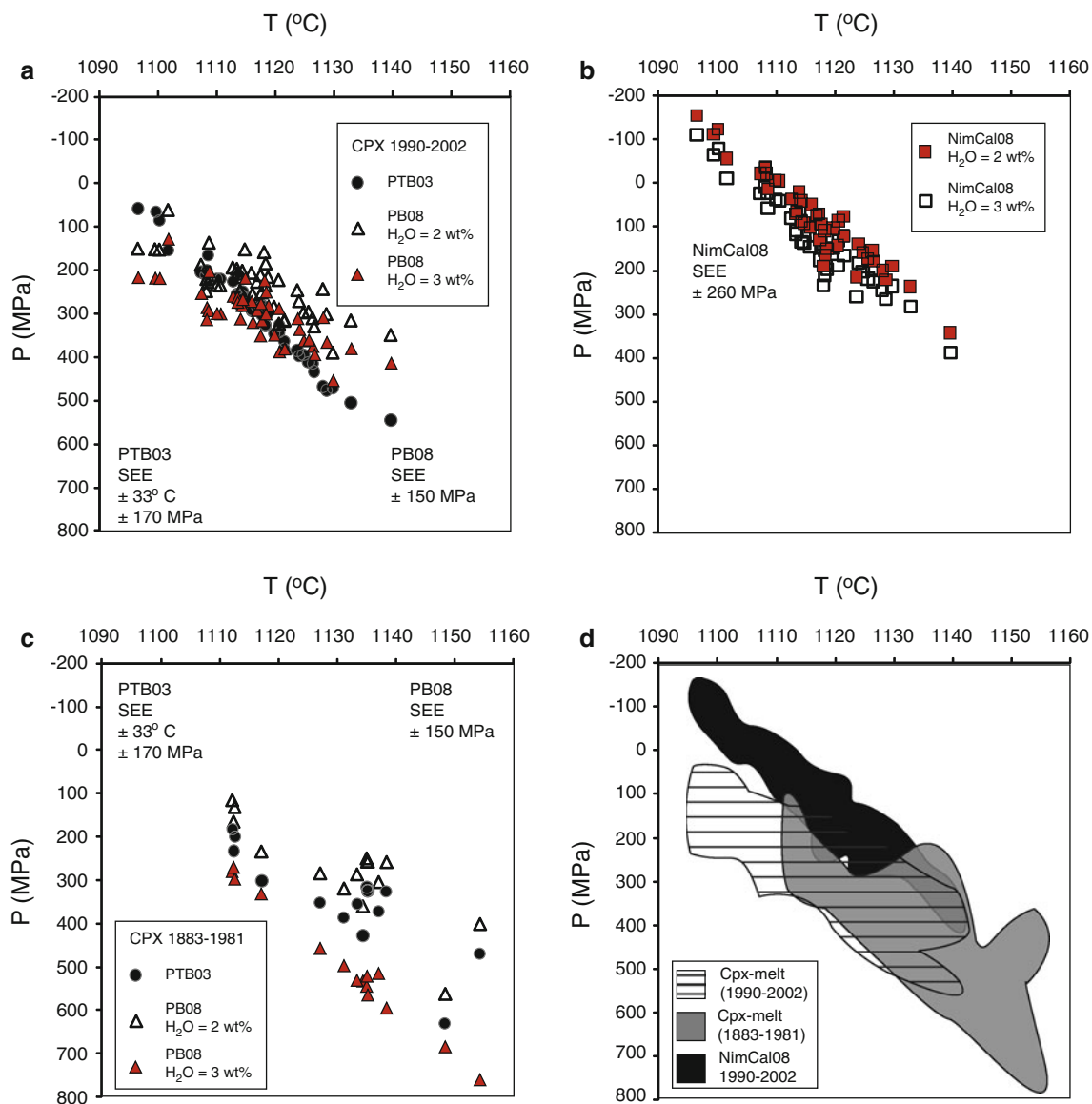


**Fig. 7** Results of PTB03 (circles), PB08 (triangles) and NimCal08 (squares) calculations. **a** PTB03 and PB08 results for clinopyroxene erupted 1990–2002. Note that the results of the PTB03 and PB08 models overlap, justifying the choice of the 1963 basalt as an appropriate equilibrium melt. SEE for PTB03 are  $\pm 33^\circ\text{C}$  and  $\pm 170$  MPa. SEE for PB08 is  $\pm 150$  MPa. **b** Results of the NimCal08

barometer partially overlap with those obtained from the PTB03 and PB08 models. SEE for NimCal08 is at 260 MPa. **c** Pressures and temperatures calculated for the older (1883–1981) clinopyroxenes are slightly higher than for the younger (1990–2002) clinopyroxenes. **d** The  $P$ – $T$  fields representing the three sets of calculated pressures and temperatures described in **a**–**c**

**Table 3** Clinopyroxene-melt thermobarometry and clinopyroxene barometry for Anak Krakatau eruptives. Calculated  $P$  and  $T$  values are given as average and range

Model	Wt% H <sub>2</sub> O	Recent clinopyroxene (1990–2002)		Older clinopyroxenes (1883–1981)	
		$P$ (MPa)	$T$ (°C)	$P$ (MPa)	$T$ (°C)
PTB03	NA	301 (58–546)	1,117 (1,097–1,140)	492 (272–759)	1,131 (1,112–1,154)
PB08	2	236 (60–389)	NA	280 (116–563)	NA
	3	303 (127–456)		347 (183–630)	
NimCal08	2	129 (–110 to 387)	NA	241 (–172 to 566)	NA
	3	84 (–155 to 342)		286 (–127 to 611)	

consistent with each other provides a strong indication that the results are reliable (cf. Longpré et al. 2008).

### Seismic tomography

In the tandem seismic tomography study (Hoffmann-Rothe et al. 2006; Jaxybulatov et al. 2011), the structure of P and S velocities as well as the distribution of Vp/Vs ratios have been obtained for the Krakatau area. The data distribution is not favourable for tomographic inversion, so thorough testing was performed to separate robust features from possible artefacts. In particular, it was shown that details of structures outside the Krakatau complex are strongly smeared and should be interpreted with prudence. At the same time, the draughtboard tests show that the shapes of the main patterns beneath the Krakatau complex, where most of the seismic events and stations are located, define real features. The amplitudes of P and S velocity anomalies were estimated using synthetic tests with realistic configurations of anomalies and noise. The general magnitudes of computed P and S anomalies beneath Krakatau are not exceptionally high, being approximately 8 and 13%, respectively. Beneath the Krakatau complex down to a depth of 5 km, higher P-velocity anomalies anticorrelate with lower S anomalies. Below 7 km depth, both P and S anomalies are negative, but the magnitude of S anomalies is much stronger. These velocity distributions result in extremely high Vp/Vs ratios (up to 2.1–2.2) in an area of ~5 km diameter beneath Anak Krakatau. In a vertical section (Fig. 10), a transition between two high Vp/Vs zones at a depth of about 7 km becomes visible. The robustness of this feature of the modelling is tested in a special synthetic model, which reveals satisfactory vertical resolution (Jaxybulatov et al. 2011). The Vp/Vs distribution in the vertical section is interpreted to reflect two distinct magma storage regions, an upper crustal one at <7 km and a mid-crustal one at >7 km. For full details on the seismic tomography, see Jaxybulatov et al. (2011).

### Discussion

Key factors controlling the ascent of silicate magmas include (a) fractures, (b) states of stress, (c) mechanical properties of the lithosphere and (d) density contrast between magma and country rock, where lower density lithologies act as barriers for denser magma (cf. Shaw 1980; Stolper and Walker 1980; Gudmundsson 1986; Kuntz 1992; Yang et al. 1999; Putirka et al. 2003). Below Anak Krakatau, the crust can be broadly divided into three main lithological packages (Fig. 2a) and is heavily fractured and faulted, making this volcano particularly well suited for investigating magma ascent and evolution.

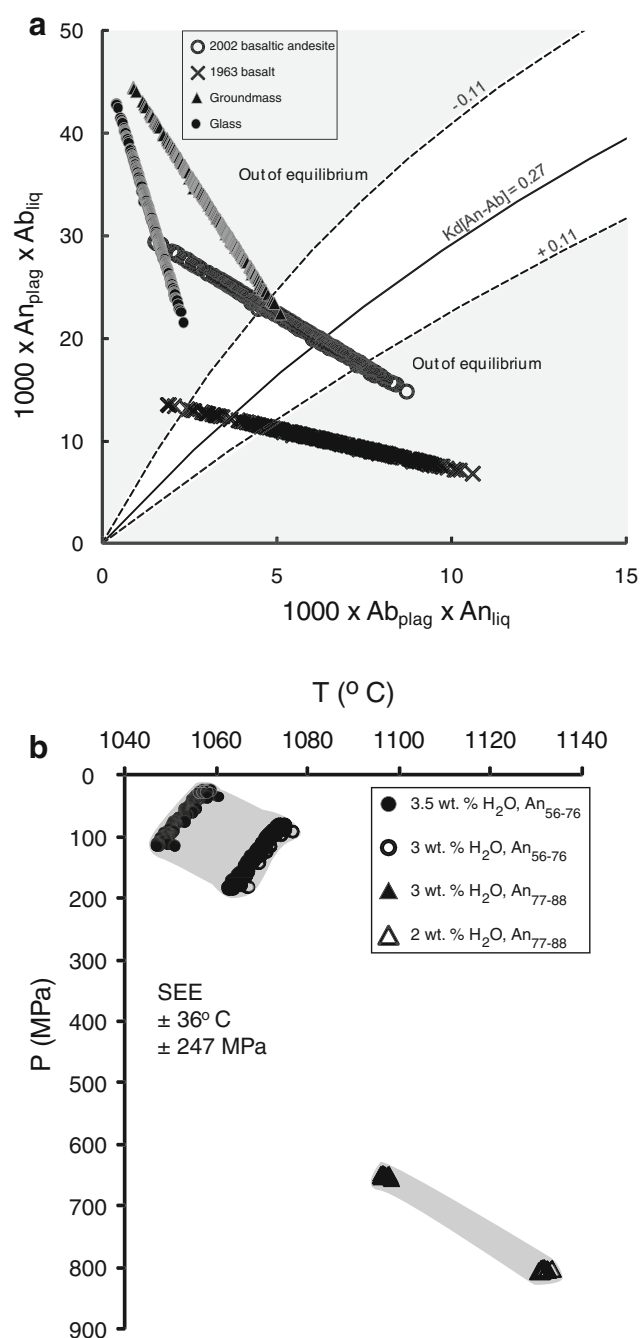


**Fig. 8** **a** Test for plagioclase and four possible equilibrium melt options. The 2002 basaltic andesite appear to be in equilibrium with medium anorthite plagioclase ( $An_{56-76}$ ), while the 1963 basalt is a better fit for the high anorthite plagioclase ( $An_{77-88}$ ). **b** Results of plagioclase-melt thermobarometry, recording two separate regions of plagioclase crystallization. Plagioclase with medium anorthite content ( $An_{56-76}$ ) records shallow crustal storage (3–7 km), while the high-anorthite plagioclase crystallized below Moho (23–28 km). SEE for the plagioclase-melt thermobarometer are  $\pm 36^\circ\text{C}$  and  $\pm 247\text{ MPa}$ , and so the results for 3 and 3.5 wt%  $\text{H}_2\text{O}$  overlap within the uncertainties

Our clinopyroxene-melt and plagioclase-melt thermobarometry produces three distinct and separate sets of  $P$ – $T$  estimates, which are also independently detected by

**Table 4** Results from plagioclase-melt thermobarometry for Anak Krakatau eruptives. Calculated  $P$  and  $T$  values are given as average and range, where appropriate

$T$ (°C)	Saturation surface $T$ (°C)	$P$ (MPa)	Wt% H <sub>2</sub> O	Nominal melt
1,053 (1,047–1,058)	1,062	70 (23–117)	3.5	2002 basaltic andesite
1,069 (1,063–1,074)	1,077	136 (81–186)	3	2002 basaltic andesite
1,098 (1,097–1,098)	1,104	651 (645–658)	3	1963 basalt
1,132 (1,131–1,133)	1,138	800 (793–807)	2	1963 basalt

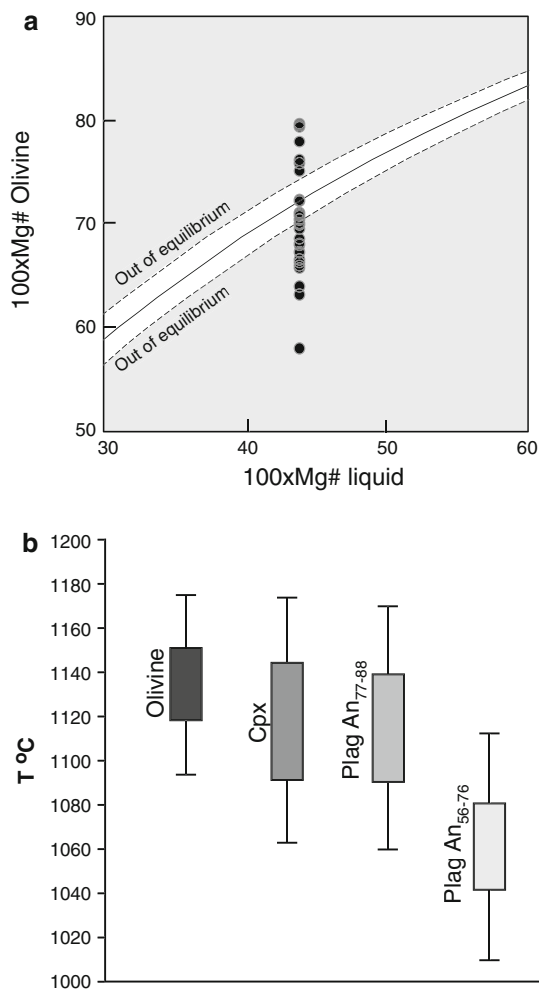


**Fig. 9** **a** Test for olivine-melt equilibrium. Only the olivines in equilibrium with the 1963 basalt (Fo<sub>70–72</sub>) are used in the calculations. **b** Results of all mineral-melt thermometers employed. The temperatures calculated using olivine-melt thermometry overlap with but are also slightly higher than the temperatures calculated for clinopyroxene as well for high-anorthite (An<sub>77–88</sub>) plagioclase, all of which are in equilibrium with the 1963 basalt. The temperatures calculated for plagioclase in equilibrium with the more evolved 2002 basaltic andesite (An<sub>56–76</sub>) are significantly lower. The SEE for olivine-melt thermometry is at  $\pm 29^\circ\text{C}$ . Also refer to Figs. 7 and 8b

seismic studies (Harjono et al. 1989; Jaxybulatov et al. 2011; this study) and are consistent with in situ crystal isotope stratigraphy (Gardner et al. in press) as well as chlorine content in melt inclusions (Mandeville et al. 1996a). This

strongly indicates three separate levels of crystallization and thus three different levels of magma storage. In Fig. 10 and Table 6, the results from plagioclase-melt and clinopyroxene-melt barometry are compared. The plagioclase crystallization is focused in the region of 3–7 (An<sub>56–76</sub>) and 23–28 (An<sub>77–88</sub>) km, while the majority of clinopyroxenes appear to have formed in the region of 7–12 km.

The large compositional variation of plagioclase (An<sub>45–90</sub>), the sieve-like textures and complex zoning patterns are features commonly observed in basaltic and andesitic, subduction-related volcanic rocks, and there is a widely held view that they reflect crystallization in a highly dynamic magma system (e.g. Tepley et al. 1999; Troll et al. 2004; Chadwick et al. 2007). Sieve-like textures may develop as a result of crystallographic-controlled dissolution of crystals in a system where the particular plagioclase composition has become unstable. This can occur by external heating to temperatures above solidus, i.e. during partial melting (e.g. Johannes et al. 1994; Petcovic and Grunder 2003; Årebäck et al. 2008), or by mixing of more Ab-rich plagioclase xenocrysts from a felsic magma into a (hotter) more mafic magma (e.g. Tsuchiyama 1985; Andersson and Eklund 1994; Hattori and Sato 1996). Alternatively, sieve-like textures may arise by rapid ‘skeletal’ growth at conditions of supersaturation due to rapid undercooling and/or mixing of two magmas to an intermediate composition (e.g. Lofgren 1974, 1980; Kuo and Kirkpatrick 1982; Landi et al. 2004; O’Driscoll et al. 2007). The most sodic plagioclase compositions (An<sub>45–55</sub>) did not equilibrate with the basaltic andesite magma, but they have compositions that overlap with those found in 1883 rhyodacite and 1981 dacite rocks (Camus et al. 1987; Mandeville et al. 1996a), suggesting a possible origin as resorbed xenocrysts from felsic volcanics and intrusives or from assimilation of felsic crust. Similarly, the most calcic plagioclase (An<sub>77–88</sub>) was equilibrated in a basaltic melt similar to the 1963 basalt rather than in a basaltic andesite, as suggested would be the case in Camus et al. (1987). Thus, textural evidence (as also discussed by Gardner et al. 2006, in press) together with the equilibrium tests suggests that although plagioclase crystals of various origins are present, only those of intermediate composition ( $\sim$ An<sub>56–76</sub>) crystallized from a melt similar in composition to that of the basaltic andesite in which they occur. The

**Table 5** Results of olivine-melt thermometry. Calculated  $T$  values are given as average and range

Model	Wt% H <sub>2</sub> O	$T$ (°C) Fo <sub>70–72</sub>
PO07	2	1,144 (1,141–1,145)
	3	1,127 (1,124–1,128)

depths calculated for crystallization of these medium-anorthite plagioclases (3–7 km) fit well with previous results of plagioclase-melt geobarometry (Camus et al. 1987; Mandeville et al. 1996a), as well as evidence from crystal isotope stratigraphy (Gardner et al. 2006, in press), and confirm the presence of a shallow magma storage region beneath Anak Krakatau. The high-anorthite plagioclase records a depth of crystallization that is very much in agreement with the sub-Moho level detected by Harjono et al. (1989).

Similarly, the zone of clinopyroxene crystallization (7–12 km) coincides with the magma chamber system identified by Harjono et al. (1989) at a depth of ~9 km (with an unknown downward extension). These contrasting depth levels calculated for plagioclase and clinopyroxene crystallization are not contradictory. In contrast, An<sub>56–76</sub> plagioclase is more likely to preserve a later stage of crystallization than clinopyroxene in mafic magmas (e.g. Bowen 1928), as is also confirmed by the observed textures

(Fig. 4d). Therefore, the results of our thermobarometry are in agreement with this order of crystallization, indicating that the late stage, medium-anorthite plagioclase forms at shallow level in the crust beneath Anak Krakatau. Harjono et al. (1989) was not able to identify a seismic attenuation zone at depths less than 9 km, but this does not exclude shallower magma storage. As discussed by Gardner et al. (2006, in press), a diffuse zone of small pockets of magma would avoid detection by a broad-scale micro-seismic study such as that of Harjono et al. (1989).

The tomography study performed in tandem with this work, in turn, detected two broad but separate crustal magma storage regions. These are constrained to depths of <7 and >7 km, respectively (Hoffmann-Rothe et al. 2006; Jaxybulatov et al. 2011) and are consistent with the upper two levels of magma storage detected by our thermobarometry investigation. The tomography study unfortunately suffered from limited resolution at depths greater than ~15 km (Jaxybulatov et al. 2011), and the very deep, sub-Moho storage region was not resolvable.

Therefore, the combined thermobarometric, geophysical and isotopic evidence point towards three distinct magma storage regions that feed Anak Krakatau: one at a depth of approximately 3–7 km (An<sub>56–76</sub> plagioclase crystallization), another at 7–12 km (clinopyroxene crystallization) and yet another very deep storage region at  $\geq 22$  km (crystallization of An<sub>77–88</sub> plagioclase and olivine).

**Fig. 10** A comparison of the results of the thermobarometry with the tandem seismic tomography study. The Vp/Vs ratio is obtained from real data inversion. Red dots represent seismic events below the Krakatau complex during the period of study. For full details, see Jaxybulatov et al. (2011). The tomography indicates two distinct magma storage regions in the crust, one above and one below approximately 7 km, which is broadly consistent with the results of the thermobarometry as both sets of results indicate the presence of shallow crustal plus mid-crustal storage regions. The sub-Moho storage region (23–28 km) detected by the thermobarometry was not detected by the tomography due to limitations in resolution for depths greater than 15 km

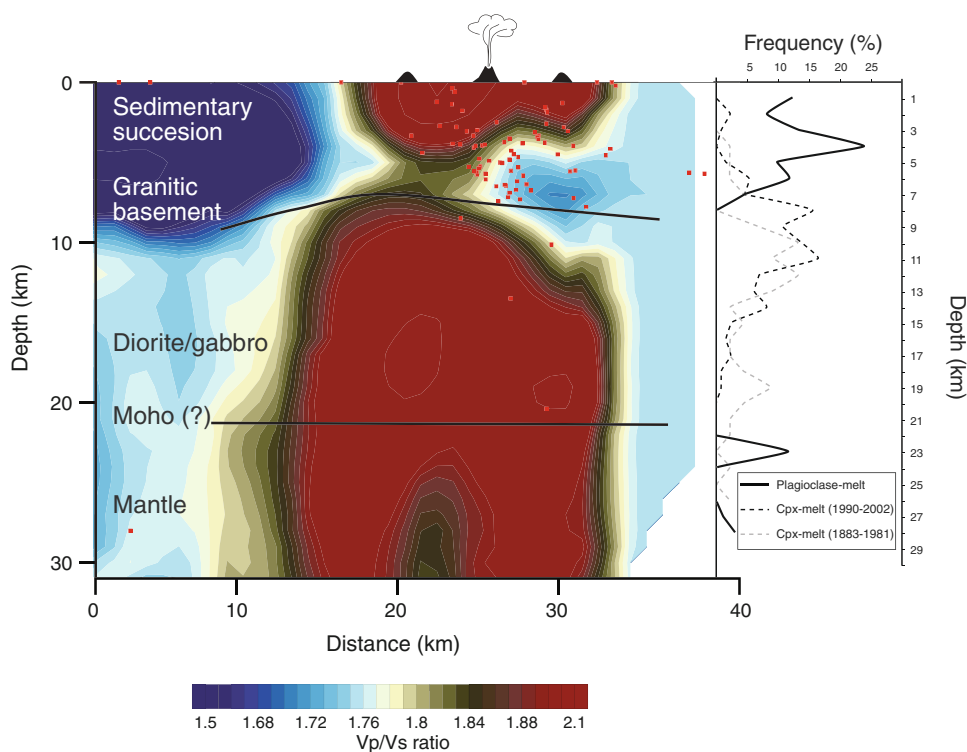


**Table 6** Calculated pressures converted to depth. Calculated depth values are given as average and range

Model	Mineral phase	Wt% H <sub>2</sub> O	Depth of crystallization (km)
PTB03	Clinopyroxene 1990–2002	NA	11.46 (2.55–19.96)
PB08	Clinopyroxene 1990–2002	2	11.59 (5.32–16.85)
		3	9.23 (2.19–14.54)
PTB03	Clinopyroxene 1883–1981	NA	18.06 (10.49–26.68)
PB08	Clinopyroxene 1883–1981	2	13.09 (7.36–22.78)
		3	10.75 (4.92–20.57)
Plagioclase-melt	Plagioclase An <sub>56–76</sub>	3	5.51 (3.60–7.40)
		3.5	2.98 (1.01–4.88)
Plagioclase-melt	Plagioclase An <sub>77–88</sub>	2	28.05 (27.98–28.12)
		3	23.37 (23.22–23.60)

### A model for Anak Krakatau

Our results and those from previous work (Camus et al. 1987; Harjono et al. 1989; Mandeville et al. 1996a; Gardner et al. 2006, *in press*; Hoffmann-Rothe et al. 2006; Jaxybulatov et al. 2011) indicate that magma emplacement and storage at Anak Krakatau volcano coincide with the major lateral lithological boundaries in the crust at 4, 9 and 22 km depth (Figs. 2a, 10). There, density contrasts between the different lithologies is likely a controlling parameter, causing ascending dense magma to stall. Below each of these lithological/density boundaries, lateral transport will cause magma pockets to grow and evolve further. The evolution of magma beneath Anak Krakatau is envisaged to have been characterized through the following stages (Fig. 11):

1. Partial melting of the mantle wedge producing a primary basaltic magma, followed by transport of magma to the mantle–crust boundary. There, magma ascent is halted due to the density contrast between the mantle and the lower crust (at ~22 km depth). The initial melt composition may be considerably influenced by decompressional melting, due to the extensional character of the Sunda Strait (Harjono et al. 1991). The extent of the seismic attenuation zone detected by Harjono et al. (1989) implies that this deep storage region is large scale and likely interconnected. This would, in part, account for the semi-continuous supply of magma to the Anak Krakatau system. Analogues to this may be the “MASH” zones proposed by Hildreth and Moorbath (1988) or the more recent “deep-crustal hot zones” proposed by e.g. Annen et al. (2006). At this level, crystallization of high-anorthite plagioclase and also olivine takes place.
2. Ascent of basalt takes place either when magma density has decreased by fractionation to below that of the lower crust (~2.95 g cm<sup>-3</sup>, Table 1) or when replenishment of fresh basalt, with associated volatile

release, into the magma chambers from below forces ascent to higher levels.

3. The ascending magma then stalls at a mid-crustal level due to the next major density contrast, this time at a depth of about 9 km (Fig. 11, granite–diorite transition), where the dominant phase of crystallization of clinopyroxene takes place. The euhedral habitus and homogenous composition of all observed and analysed clinopyroxenes would indicate a sizeable and stable storage region with a semi-continuous supply of magma. The bulk composition of the magma at this level is likely close to the evolved basalt documented in Zen and Hadikusumo (1964), as indicated by clinopyroxene being in apparent equilibrium with this composition at the calculated thermodynamic conditions (Fig. 6). Interestingly, Camus et al. (1987) noted that the composition of the clinopyroxenes found in the 1981 acidic-andesites does not differ significantly from those in the basaltic andesites, implying a common source for the clinopyroxenes, despite differences in host rock chemistry of different eruptions.
4. Further ascent of magma is triggered by continued crystal fractionation (and possibly also assimilation/mixing with felsic crust/magmas), shifting the magma towards yet lower density (e.g. basaltic andesite composition) until that of the middle crust (~2.75 g cm<sup>-3</sup>) is approached. After this, magma will begin to rise again. Alternatively, replenishment with fresh magma and associated release of gases from below may help force ascent.
5. At a depth of ~4 km, the magma ascent is stalled once more, this time at the granite-sedimentary lithological boundary (Fig. 11). A major phase of An<sub>56–76</sub> plagioclase crystallization takes place at this level. This shallow storage region is likely made up of a plexus of more or less interconnected pockets of magma dispersed in the crust, as it was not detected in the low resolution micro-seismic study of Harjono et al.

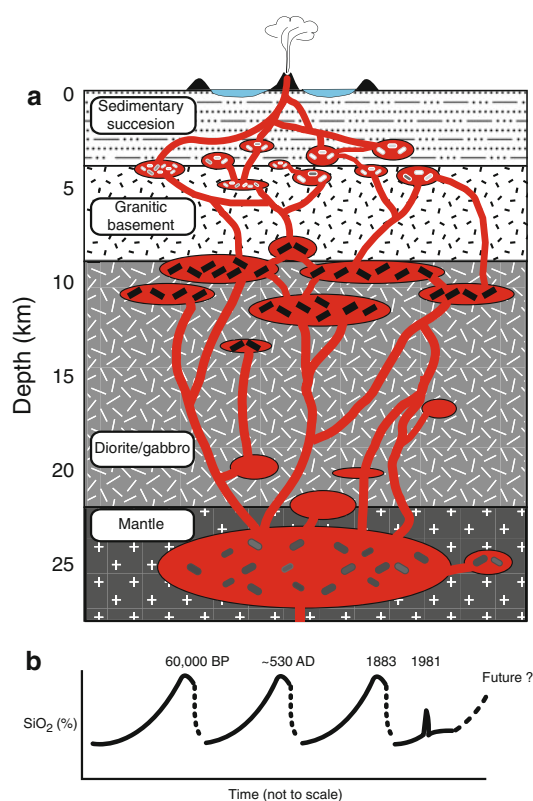


**Fig. 11** **a** Schematic illustration of the magma plumbing system at Anak Krakatau based on thermobarometric and geophysical data. **b** Eruption cyclicity of Krakatau, redrawn and modified from van Bemmelen (1949). Since the ignimbrite eruption in 1883, all analysed rocks erupted from Anak Krakatau have been of basaltic or basaltic andesite composition, with the notable exception of a single event in 1981, when acidic-andesites were erupted

(1989). In contrast, the seismic tomography reported here appears to pick up signals of this shallow storage level (cf. Hoffmann-Rothe et al. 2006; Jaxybulatov et al. 2011). It is at this level that magma evolves to its final pre-eruptive composition (i.e. evolved basaltic andesite), as indicated by the late-crystallized plagioclase of intermediate composition being in equilibrium with this bulk composition at the calculated thermodynamic conditions.

Thermal preconditioning of the upper crust by mafic to intermediate magmas has been suggested to be a major factor in the production of rhyolitic magmas (e.g. Troll et al. 2004; Price et al. 2005; Annen et al. 2006). Such a petrogenetic model could be applicable to the Krakatau complex, considering its history of recurring major dacitic-rhyolitic eruptions with intermittent periods of mafic to intermediate magmatism. A steep geothermal gradient and continuous heating of the crust eventually leads to large-scale assimilation of country rock, as well as partial melting and recycling of comagmatic intrusives. The idea that the uppermost magma storage region detected (~3 to

7 km) is currently made up of a plexus of magma pockets resulting in a very high surface-to-volume ratio of the stored magma at that depth would implicate an efficient heat transfer from magma to crust. The high magma throughput at Anak Krakatau, evident in the average extrusive growth of ~7.5 cm/week, adds to the efficient heating of the crust. The geothermal gradient in one of the 3-km-deep wells, about 30 km south-southeast of Krakatau, has been estimated to be as high as 67°C/km (Nishimura et al. 1986). With the model proposed by Price et al. (2005) and the cyclicity of van Bemmelen (1949) (Fig. 11b) in mind, the possible shallowing of the plumbing system detected in this study (Fig. 7c) could be an indication that Krakatau is again in the process of evolving towards a larger and higher silica system culminating in a major explosive eruption. Therefore, continuous seismic and petrological monitoring of Anak Krakatau remains of utmost relevance. This is especially true considering that Indonesia today has the world's fourth largest population, with a much more densely populated proximal area compared with that in 1883 when the latest major ignimbrite eruption claimed 36,000 lives.

## Conclusions

Recent magmas erupted from Anak Krakatau record clinopyroxene crystallization at mid-crustal level (7–12 km), within a magma storage region previously identified in micro-seismic and tomographic studies (Harjono et al. 1989; Jaxybulatov et al. 2011). In contrast, plagioclase records both sub-Moho (23–28 km) and upper crustal (3–7 km) depths of crystallization. High-anorthite plagioclase ( $An_{77-88}$ , 11% of datapoints), in equilibrium with a basaltic melt, forms at approximately the crust-mantle interface, coinciding with the deep storage region detected in Harjono et al. (1989). The much more abundant medium-anorthite plagioclase ( $An_{56-76}$ , 68% of datapoints), in equilibrium with a basaltic andesite melt, forms in the upper crust, in agreement with the upper storage region detected by Jaxybulatov et al. (2011). This is also in agreement with previous estimates based on plagioclase barometry, chlorine in fluid inclusions barometry and supported by crystal isotope stratigraphy (Camus et al. 1987; Mandeville et al. 1996a; Gardner et al. 2006, *in press*).

The magma storage regions detected beneath Krakatau coincide with major lithological boundaries in the crust, implying that magma ascent at Anak Krakatau is in part controlled by lateral crustal discontinuities. This, in turn, indicates that, at this volcano, density contrast between magma and bedrock is an important parameter for magma ascent. Additionally, the extensional character and heavily

faulted bedrock in the Sunda Straits (Nishimura et al. 1986) are likely fundamental in providing vertical pathways for magma ascent.

Our study demonstrates that petrology is able to detect magma storage zones in the crust where conventional seismic surveys (e.g. Harjono et al. 1989) fail due to limitations in resolution (e.g. the shallow reservoir below Anak Krakatau). In contrast, seismic surveys may pick up signals of deeper storage regions from which none of the appropriate phenocryst phases remain in the eruptive products. This may be due to e.g. cumulate capture, resorption and/or replacement of minerals. Combined geophysical and petrological surveys thus offer the highest potential for a thorough characterization of magma plumbing at active volcanic complexes.

**Acknowledgments** We thank Dr. Keith D. Putirka, who provided valuable help with our questions on the thermobarometric models and calibrations. We are grateful to Lara Blythe, Frances Deegan, Lothar Schwarzkopf, David Hilton, Lilli Freda and Piergiorgio Scarlato for help during fieldwork. The project was supported by Science Foundation Sweden (Vetenskapsrådet), Uppsala University and the Otterborgs donationsfond.

## References

- Andersson UB (1997) Petrogenesis of some Proterozoic granitoid suites and associated basic rocks in Sweden (geochemistry and isotope geology). *SGU Rapp & Medd* 91:216
- Andersson UB, Eklund O (1994) Cellular plagioclase intergrowths as a result of crystal-magma mixing in the Proterozoic Åland rapakivi batholith, SW Finland. *Contrib Mineral Petrol* 117:124–136
- Annen C, Blundy JD, Sparks RSJ (2006) The genesis of intermediate and silicic magmas in deep crustal hot zones. *J Petrol* 47:505–539
- Årebäck H, Andersson UB, Petersson J (2008) Petrological evidence for crustal melting, unmixing, and undercooling in an alkali-calcic, high-level intrusion: the late Sveconorwegian Vinga intrusion, SW Sweden. *Mineral Petrol* 93:1–46
- Barker AK, Holm PM, Peate DW, Baker JA (2009) Geochemical stratigraphy of submarine lavas (3–5 Ma) from the Flamengos Valley, Santiago, Southern Cape Verde Islands. *J Petrol* 50:169–193
- Bowen NL (1928) *The evolution of the igneous rocks*. Princeton University Press, Princeton, p 334
- Camus G, Gourgaud A, Vincent PM (1987) Petrologic evolution of Krakatau (Indonesia): implications for a future activity. *J Volcanol Geotherm Res* 33:299–316
- Caprarelli G, Riedel SP (2005) A clinopyroxene–basalt geothermobarometry perspective of Columbia Plateau (NW-USA) Miocene magmatism. *Terra Nova* 17:265–277
- Cashman KV (1990) Textural constraints on the kinetics of crystallization of igneous rocks. In: Nicholls J, Russell JK (eds) *Modern methods of igneous petrology: understanding magmatic processes*. *Mineral Soc Am Rev Mineral* 24:259–314
- Chadwick JP, Troll VR, Ginibre C, Morgan D, Gertisser R, Waight TE, Davidson JP (2007) Carbonate assimilation at Merapi Volcano, Java, Indonesia: insights from crystal isotope stratigraphy. *J Petrol* 48:1793–1812
- Deplus C, Bonvalot S, Dahrin D, Diament M, Harjono H, Dubois J (1995) Inner structure of the Krakatau volcanic complex (Indonesia) from gravity and bathymetry data. *J Volcanol Geotherm Res* 64:23–52
- Devine JD, Gardner JE, Brack HP, Layne GD, Rutherford MJ (1995) Comparison of microanalytical methods for estimating H<sub>2</sub>O contents of silicic volcanic glasses. *Am Mineral* 80:319–328
- Duke JM (1976) Distribution of the period four transition elements among olivine, calcic clinopyroxene and mafic silicate liquid: experimental results. *J Petrol* 17:499–521
- Galipp K, Klügel A, Hansteen TH (2006) Changing depths of magma fractionation and stagnation during the evolution of an oceanic island volcano: La Palma (Canary Islands). *J Volcanol Geotherm Res* 155:258–306
- Gardner MF, Troll VR, Hart G, Gertisser R, Wolf JA, Gamble JA (2006) Shallow-level processes at Anak Krakatau: crystallisation and late stage crustal contamination. *Goldschmidt conference abstracts A194*
- Gardner MF, Troll VR, Gamble JA, Gertisser R, Hart GL, Ellam RM, Harris C, Wolf JA (in press) Shallow level differentiation processes at Krakatau: evidence for late-stage crustal contamination. *J Petrol*
- Ghiorso MS, Hirschmann MM, Reiners PW, Kress VCI (2002) The pMELTS: a revision of MELTS for improved calculation of phase relations and major element partitioning related to partial melting of the mantle to 3 GPa. *Geochem Geophys Geosystems* 3. doi:10.1029/2001GC000217
- Gudmundsson A (1986) Formation of crustal magma chambers in Iceland. *Geology* 14:164–166
- Hamilton WB (1979) *Tectonics of the Indonesian region*. United States Geological Survey Professional Paper 1078
- Harjono H, Diament M, Nouaili L, Dubois J (1989) Detection of magma bodies beneath Krakatau volcano (Indonesia) from anomalous shear waves. *J Volcanol Geotherm Res* 39:335–348
- Harjono H, Diament M, Dubois J, Larue M (1991) Seismicity of the Sunda Strait: evidence for crustal extension and volcanological implications. *Tectonics* 10:17–30
- Hattori K, Sato H (1996) Magma evolution recorded in plagioclase zoning in 1991 Pinatubo eruption products. *Am Mineral* 81:982–994
- Hildreth W, Moorbath S (1988) Crustal contributions to arc magmatism in the Andes of Central Chile. *Contrib Mineral Petrol* 98:455–489
- Hoffmann-Rothe A, Ibs-von Seth M, Kneiß R, Faber E, Klinge K, Reichert R (2006) Monitoring Anak Krakatau volcano in Indonesia. *EOS* 87:581–586
- Housh TB, Luhr JF (1991) Plagioclase-melt equilibria in hydrous systems. *Am Mineral* 76:477–492
- Ibs-von Seht M (2008) Detection and identification of seismic signals recorded at Krakatau volcano (Indonesia) using artificial neural networks. *J Volcanol Geotherm Res* 176:448–456
- Jarrard RD (1986) Relations among subduction parameters. *Rev Geophys* 24:217–284
- Jaxybulatov K, Koulakov I, Ibs-von Seht M, Klinge K, Reichert C, Dahren B, Troll VR (2011) Evidence for high fluid/melt content beneath Krakatau volcano (Indonesia) from local earthquake tomography. *J Volcanol Geotherm Res* 206:96–105
- Johannes W, Koepke J, Behrens H (1994) Partial melting reactions of plagioclase and plagioclase-bearing systems. In: Parson I (ed) *Feldspars and their reactions*. Kluwer, Dordrecht, pp 161–194
- Judd JW (1889) The earlier eruptions of Krakatau. *Nature* 40:365–366
- Klügel A, Klein F (2005) Complex magma storage and ascent at embryonic submarine volcanoes from the Madeira Archipelago. *Geology* 34:337–340
- Klügel A, Hansteen TH, Galipp K (2005) Magma storage and underplating beneath Cumbre Vieja volcano, La Palma (Canary Islands). *EPSL* 236:211–226

- Kopp H, Flueh ER, Klaeschen D, Bialas J, Reichert C (2001) Crustal structure of the central Sunda margin at the onset of oblique subduction. *Geophys J Int* 147:449–474
- Koulakov I (2009) LOTOS code for local earthquake tomographic inversion: benchmarks for testing tomographic algorithms. *Bull Seismol Soc Am* 99:194–214
- Kudo AM, Weill DF (1970) An igneous plagioclase thermometer. *Contrib Mineral Petrol* 25:52–65
- Kuntz M (1992) A model-based perspective of basaltic volcanism, eastern Snake River Plain, Idaho. In: Link PK, Kuntz MA, Plat LB (eds) *Regional geology of eastern Idaho and Western Wyoming*. *Geol Soc Am Memoir* 179:289–304
- Kuo LC, Kirkpatrick RJ (1982) Pre-eruption history of phyric basalts from DSDP legs 45 and 46: evidence from morphology and zoning patterns in plagioclase. *Contrib Mineral Petrol* 79:13–27
- Landi P, Métrich N, Bertagnini A, Rosi M (2004) Dynamics of magma mixing and degassing recorded in plagioclase at Stromboli (Aeolian Archipelago, Italy). *Contrib Mineral Petrol* 147:213–227
- le Bas MJ, le Maitre RW, Streckeisen A, Zanettin B (1986) A chemical classification of volcanic rocks based on the total alkali-silica diagram. *J Petrol* 27:745–750
- Lelgemann H, Gutscher M, Bialas J, Flueh E, Weinrebe W, Reichert C (2000) Transtensional basins in the western Sunda Strait. *Geophys Res Lett* 27:3545–3548
- Lofgren GE (1974) An experimental study of plagioclase crystal morphology: isothermal crystallization. *Am J Sci* 274:243–273
- Lofgren GE (1980) Experimental studies on the dynamic crystallization of silicate melts. In: Hargraves RB (ed) *Physics of magmatic processes*. Princeton University Press, Princeton
- Longpré MA, Troll VR, Hansteen TH (2008) Upper mantle magma storage and transport under a Canarian shield-volcano, Teno, Tenerife (Spain). *J Geophys Res* 113. doi:10.1029/2007JB005422
- Lunt P, Burgon G, Baky A (2009) The Pemali formation of Central Java and equivalents: indicators of sedimentation on an active plate margin. *J Asian Earth Sci* 34:100–113
- Mandeville CW, Carey S, Sigurdsson H (1996a) Magma mixing, fractional crystallization and volatile degassing during the 1883 eruption of Krakatau volcano, Indonesia. *J Volcanol Geotherm Res* 74:243–274
- Mandeville CW, Carey S, Sigurdsson H (1996b) Sedimentology of the Krakatau 1883 submarine pyroclastic deposits. *Bull Volcanol* 96:512–529
- Métrich N, Rutherford MJ (1992) Experimental study of chlorine behaviour in hydrous silicic melts. *Geochim Cosmochim Acta* 56:607–616
- Mordick BE, Glazner AF (2006) Clinopyroxene thermobarometry of basalts from the Coso and Big Pine volcanic fields, California. *Contrib Mineral Petrol* 152:111–124
- Morimoto N, Fabries J, Ferguson AK, Ginzburg IV, Ross M, Seifert FA, Zussman J, Aoki K, Gottardi G (1988) Nomenclature of pyroxenes. *Mineral Petrol* 39:55–76
- Nimis P (1995) A clinopyroxene geobarometer for basaltic systems based on crystal-structure modelling. *Contrib Mineral Petrol* 121:115–125
- Nimis P (1999) Clinopyroxene geobarometry of magmatic rocks. Part 2. Structural geobarometers for basic to acid, tholeiitic and mildly alkaline magmatic systems. *Contrib Mineral Petrol* 135:62–74
- Nimis P, Ulmer P (1998) Clinopyroxene geobarometry of magmatic rocks Part 1: an expanded structural geobarometer for anhydrous and hydrous, basic and ultrabasic systems. *Contrib Mineral Petrol* 133:122–135
- Ninkovich D (1976) Late Cenozoic clockwise rotation of Sumatra. *EPSL* 29:269–275
- Ninkovich D (1979) Distribution, age and chemical composition of tephra layers in deep-sea sediments off western Indonesia. *J Volcanol Geotherm Res* 5:67–86
- Nishimura S, Harjono H (1992) The Krakatau Islands: the geotectonic setting. *GeoJournal* 28:87–98
- Nishimura S, Nishida J, Yokoyama T, Hehuwat F (1986) Neotectonics of the Straits of Sunda, Indonesia. *J Southeast Asian Earth Sci* 1:81–91
- Noujiam A (1976) Drilling in a high temperature and overpressured area Sunda Straits, Indonesia. In: *Proceedings of the fifth annual convention, Indonesian Petroleum Association, Jakarta*, pp 211–214
- Ōba N, Tomita K, Yamamoto M, Istidjab M, Badruddin M, Parlin M, Sadjiman, Djuwandi A, Sudradjat A, Suhanda T (1983) Geochemical study of lava flows, ejecta and pyroclastic flows from the Krakatau group, Indonesia. *Rept Fac Sci Kagoshima Univ* 16:21–41
- O'Driscoll B, Donaldson CH, Troll VR, Jerram DA, Emeleus CH (2007) An origin for harrisitic and granular olivine in the Rum Layered Suite, NW Scotland: a crystal size distribution study. *J Petrol* 48:253–270
- Petcovic HL, Grunder AL (2003) Textural and thermal history of partial melting in tonalitic wallrock at the margin of a basalt dike, Wallowa Mountains, Oregon. *J Petrol* 44:2287–2312
- Price RC, Gamble JA, Smith IEM, Stewart RB, Eggins S, Wright IC (2005) An integrated model for the temporal evolution of andesites and rhyolites and crustal development in New Zealand's North Island. *J Volcanol Geotherm Res* 140:1–24
- Putirka KD (1999) Clinopyroxene + liquid equilibrium to 100 kbar and 2450 K. *Contrib Mineral Petrol* 135:151–163
- Putirka KD (2005) Igneous thermometers and barometers based on plagioclase + liquid equilibria: test of some existing models and new calibrations. *Am Mineral* 90:336–346
- Putirka KD (2008) Thermometers and barometers for volcanic systems. In: Putirka KD, Tepley FE (eds) *Rev Mineral Geochem* 69:61–120
- Putirka KD, Condit C (2003) A cross section of a magma conduit system at the margins of the Colorado Plateau. *Geology* 31:701–704
- Putirka KD, Mikaelian H, Ryerson F, Shaw H (2003) New clinopyroxene-liquid thermobarometers for mafic, evolved, and volatile-bearing lava compositions, with applications to lavas from Tibet and the Snake River Plain, Idaho. *Am Mineral* 88:1542–1554
- Putirka KD, Perfit M, Ryerson FJ, Jackson MG (2007) Ambient and excess mantle temperatures, olivine thermometry, and active vs. passive upwelling. *Chem Geol* 241:177–206
- Rhodes JM, Dungan MA, Blanchard DP, Long PE (1979) Magma mixing at mid-ocean ridges: evidence from basalts drilled near 22°N on the mid-atlantic ridge. *Tectonophysics* 55:35–61
- Roeder PL, Emslie RF (1970) Olivine-liquid equilibrium. *Contrib Mineral Petrol* 29:275–289
- Schlüter HU, Gaedicke C, Roeser HA, Schreckenberger B, Meyer H, Reichert C, Djajadihadja Y, Prexl A (2002) Tectonic features of the southern Sumatra-western Javan forearc of Indonesia. *Tectonics* 21. doi:10.1029/2001TC901048
- Schwarz S, Klügel A, Wohlgemuth-Ueberwasser C (2004) Melt extraction pathways and stagnation depths beneath the Madeira and Desertas rift zones (NE Atlantic) inferred from barometric studies. *Contrib Mineral Petrol* 147:228–240
- Self S (1982) Krakatau revisited: the course of events and interpretation of the 1883 eruption. *GeoJournal* 28:109–121
- Shaw HR (1980) The fracture mechanisms of magma transport from the mantle to the surface. In: Hargraves RB (ed) *Physics of magmatic processes*. Princeton University Press, Princeton, pp 201–264

- Shaw CSJ, Klügel A (2002) The pressure and temperature conditions and timing for glass formation in mantle-derived xenoliths from Baarley, West Eifel, Germany: the case for amphibole breakdown, lava infiltration and mineral-melt reactions. *Mineral Petrol* 74:163–187
- Siebert L, Simkin T (2002) *Volcanoes of the world: an illustrated catalog of Holocene volcanoes and their eruptions*. Smithsonian Institution, Global Volcanism Program, Digital Information Series, GVP-3 (<http://www.volcano.si.edu/world/>)
- Špičák Ā, Václav H, Vaněk J (2002) Seismic activity around and under Krakatau volcano, Sunda arc: constraints to the source region of island arc volcanics. *Stud Geophys Geod* 46:545–565
- Stehn CE (1929) The geology and volcanism of the Krakatau group. In: *Guidebook for 4th Pacific Science Congress*, pp 1–55
- Stolper E, Walker D (1980) Melt density and the average composition of basalt. *Contrib Mineral Petrol* 74:7–12
- Sugawara T (2001) Ferric iron partitioning between plagioclase and silicate liquid: thermodynamics and petrological applications. *Contrib Mineral Petrol* 141:659–686
- Susilohadi S, Gaedicke C, Djajadihardja D (2009) Structures and sedimentary deposition in the Sunda Strait, Indonesia. *Tectonophysics* 467:55–71
- Tepley FJ III, Davidson JP, Clyne MA (1999) Magmatic interactions as recorded in plagioclase phenocrysts of Chaos Crags, Lassen Volcanic Centre, California. *J Petrol* 40:787–806
- Tregoning P, Brunner FK, Bock Y, Puntodewo SSO, McCaffrey R, Genrich JF, Calais E, Rais J, Subarya C (1994) First geodetic measurement of convergence across the Java Trench. *Geophys Res Lett* 21:2135–2138
- Troll VR, Donaldson CH, Emeleus CH (2004) Pre-eruptive magma mixing in ash-flow deposits of the tertiary Rum Igneous Centre, Scotland. *Contrib Mineral Petrol* 147:722–739
- Tschiyama A (1985) Dissolution kinetics of plagioclase in the melt of the system diopside-albite-anorthite, and origin of dusty plagioclase in andesites. *Contrib Mineral Petrol* 89:1–16
- van Bemmelen R (1949) *The geology of Indonesia*. Government Printing Office, The Hague
- Wohletz KH (2000) Were the dark ages triggered by volcano-related climate changes in the 6th century? *EOS* 48:F1305
- Yang H-J, Frey FA, Clague DA, Garcia MO (1999) Mineral chemistry of submarine lavas from Hilo Ridge, Hawaii: implications for magmatic processes within Hawaiian rift zones. *Contrib Mineral Petrol* 135:355–372
- Zen MT, Hadikusumo D (1964) Recent changes in the Anak Krakatau Volcano. *Bull Volcanol* 27:259–268